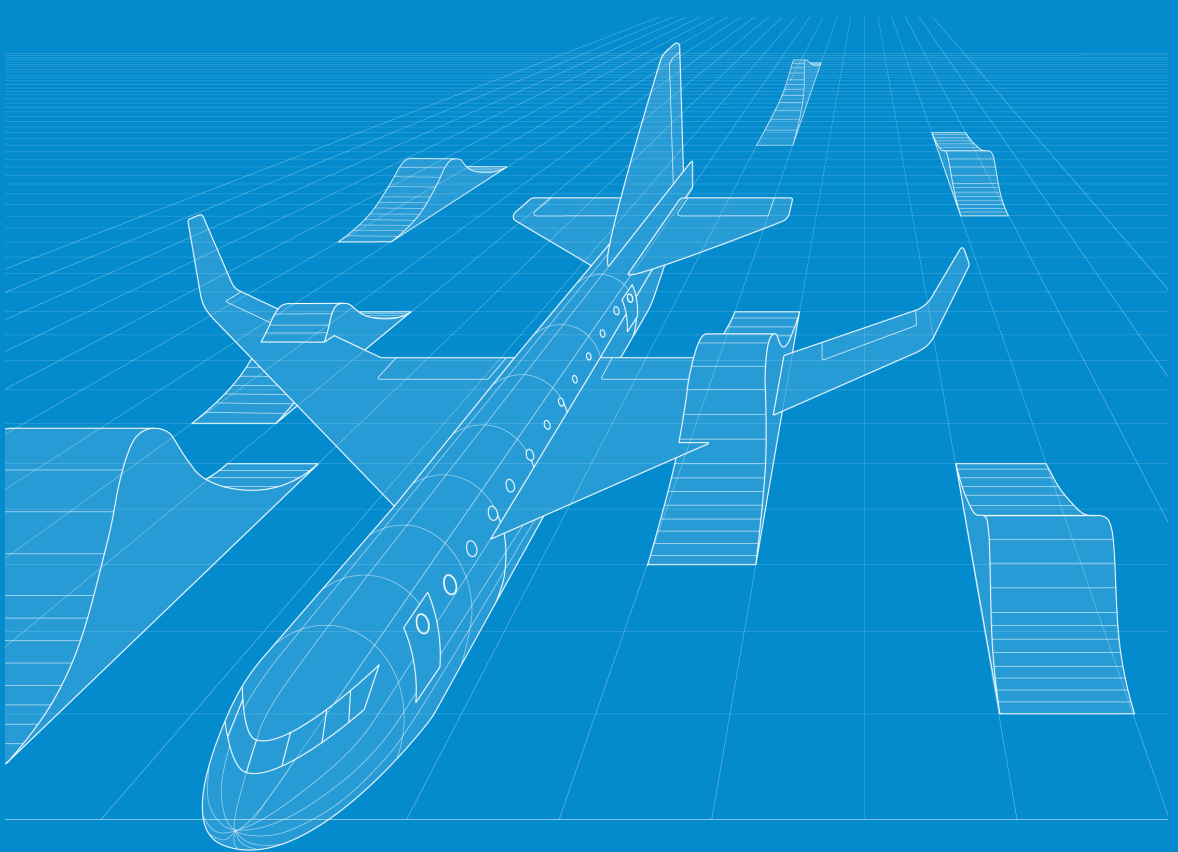


Design Guidelines for Gust Load Inclusion in Aeroelastic Optimization of a Civil Aircraft in the Preliminary Design Phase

R. Isacco

Faculty of Aerospace Engineering
Flight Performance and Propulsion



DESIGN GUIDELINES FOR GUST LOAD INCLUSION IN AEROELASTIC OPTIMIZATION OF A COMMERCIAL AIRCRAFT AT PRELIMINARY SIZING PHASE

by

Roberto ISACCO

4746740

in partial fulfillment of the requirements for the degree of

Master of Science

in Aerospace Engineering

Flight Performance and Propulsion track,

at the Delft University of Technology,

to be defended publicly on 11 November, 2019 at 13:00.

Thesis committee:	Prof.dr.ir. L.L.M. Veldhuis	TU Delft, FPP, Chair Flight Performance
	Dr.ir. R. De Breuker	TU Delft, ASM, Supervisor
	Dr.-Ing. S.G.P. Castro	TU Delft, ASM
	Ir. P. Lancelot	TU Delft, ASM

Our deepest fear is not that we are inadequate. Our deepest fear is that we are powerful beyond measure. It is our light, not our darkness, that most frightens us. Your playing small does not serve the world. There is nothing enlightened about shrinking so that other people won't feel insecure around you. We are all meant to shine as children do. It's not just in some of us; it is in everyone. And as we let our own lights shine, we unconsciously give other people permission to do the same. As we are liberated from our own fear, our presence automatically liberates others.

Tim Cruz, "Coach Carter" (2005)

ACKNOWLEDGEMENTS

The following MSc thesis is the result of a long journey, made by ups and down, hard-work, technical and attitudinal challenges. To accomplish the result that lays in front of your eyes, the support of some people has been fundamental.

To Roeland and Paul, guides of this path. Thanks for your suggestions and considerations that have been essential to realize this work.

To my family. Thanks for being always present for me, despite the distance.

To my father, reference point to me. Thanks for making this experience possible.

A mia madre, che non chiede mai ma é presenza insostituibile nella mia vita.

A Jordan e Lorenzo, compagni di avventure e sventure, la cui amicizia ha un valore inestimabile. Grazie per esserci sempre stati nonostante la distanza.

Para Pablo, fantástico compañero de casa. Gracias por aguantarme en todos los momentos de euforia y tristeza.

To Filippo. You have been like an older brother (or a grandpa) during this experience.

To Johannes. Studying and skiing friend. Thanks for your pannukakku.

A Andrea, Joshua, Niccolò, Matteo, Piero e Stefano, compagni di vita. Grazie per farmi sentire il calore (tipicamente non ligure) ovunque ci incontriamo nel mondo.

To Savastano's, Vitale's and Nugteren's families. Thanks for being always like a second family for me.

To Jaime, Steph, Tino, Tomas, Tony and all my friends in Delft. Thanks for making my time-off memorable. Sharing the struggle of the thesis with you has been a pleasure.

A Simone, Giorgio, Jurgen e tutti gli amici trinesi. Vi ringrazio di farmi sentire sempre a casa ogni volta che ci vediamo nonostante le mie lunghe assenze.

Finally, thanks to Germana and Edoardo, devoted siblings. A dedication to you to remind that even if our careers drove us apart, you will have always a reserved place in my heart.

ABSTRACT

Fundamental phase in the preliminary sizing process of an aircraft is the load case choice. Indeed, the designer, by defining which type of manoeuvres and flight conditions the aeroplane must be able to face safely, sizes the structural elements of the wing. Historically, the manoeuvres have been considered as the principal critical loads of the aircraft since they generate higher loads with respect to wind gusts or other types of wing loading situations. Moreover, the wind gust is an intrinsically dynamic phenomenon and thus more computationally expensive to analyze. However, gusts are a critical certification requirement which is becoming more and more demanding with the introduction of composite materials and high aspect ratio aircraft.

The gust load analysis is nowadays mainly included in the aeroelastic optimization of an aircraft according to certification regulations for industrial designs and to the discretion of the researcher for academic ones. The gust is therefore typically included as a static load to reduce the impact on the optimization computational costs. There is indeed an absence of methodical ways to take decisions regarding including the gust loads into the optimization and which gust model should be used in conceptual design.

This MSc thesis aims to define design guidelines for gust loads inclusion in aeroelastic optimization for the civil transport aircraft category. Several optimization cases are computed varying main design parameters, materials and gust models to understand the sensitivity of the design to the gust response analysis. The chosen aeroelastic framework is the in-house tool PROTEUS, developed by R. De Breuker et al. at the Delft University of Technology.

CONTENTS

Acknowledgements	v
Abstract	vii
Nomenclature	xi
List of Figures	xiii
List of Tables	xv
1 Introduction	1
2 Problem Statement	5
3 Literature review	7
3.1 Aeroelastic optimization: state of the art	7
3.1.1 Aircraft modelling	8
3.1.2 Load cases choice and optimization set up.	10
3.2 Gust modelling	12
3.3 Wing optimization using gust loads.	14
3.4 Analysis.	16
4 Methodology	19
5 Optimization framework	21
5.1 Pre-processor: Aircraft generator tool.	21
5.2 Aeroelastic framework: PROTEUS	25
5.3 Outer-loop of PROTEUS.	32
6 Optimization setup	35
6.1 Load cases	35
6.2 Design variables	37
6.3 Objective and constraints.	40
6.4 Optimization cases	41
7 Parametric analysis results	43
7.1 Leading-edge sweep angle	43
7.2 Wingspan	45
7.3 Maximum take-off weight.	48
7.4 Materials	50
7.5 Different gust analysis inclusions	52

8	Design guidelines and case studies	55
8.1	Design guidelines	55
8.2	Case studies.	57
9	Conclusion and recommendations	61
A	Aircraft generator: formulae and empirical studies	63
A.1	TLRs derivation	63
A.2	Performances calculation.	64
A.3	Geometry calculation	65
A.4	Weights estimation	65
A.5	Rest of the calculations	66
B	Optimization cases listed	69
C	Additional results of the parametric analysis	73
	Bibliography	77

NOMENCLATURE

Acronyms and abbreviations

AICs	Aerodynamic influence coefficients
AR	Aspect ratio
CD	Drag coefficient
CFD	Computational fluid dynamics
CL	Lift coefficient
CRM	Common research model
disp.	Displacement
DLM	Doublet lattice method
DOF	Degree of freedom
EAS	Equivalent air speed
err.	Error
ESL	Equivalent static load
FEM	Finite element method
GLA	Gust load alleviation
LE	Leading-edge
MAC	Modal assurance criterion
mac	Mean aerodynamic chord
MLG	Main landing gear
MTOW	Maximum take-off weight
norm.	Normalized
RBM	Root bending moment
reg.	Regions
SF	Safety factor
SFC	Specific fuel consumption
TAS	True air speed
TLR	Top-level requirements
UVLM	Unsteady vortex lattice method

List of symbols

\bar{A}	Ratio of root mean square of load over velocity
η	Normalized spanwise position
Λ	Sweep angle
ρ	Density
\underline{C}	Damping matrix
\underline{K}	Stiffness matrix
\underline{M}	Mass matrix
\underline{d}	Vector of displacements
\underline{q}	Generalized coordinates vector
\underline{s}	Equivalent static loads

b	Wingspan
c	Mean aerodynamic chord
$C_{L\alpha}$	Lift curve slope
D	Drag force
d	Vertical displacement
e	Oswald efficiency number
F	Force
g	Gravity acceleration
H	Half gust length
h	Flight altitude
K_g	Gust alleviation factor
L	Lift force
M	Mach number
n	Loading factor
P_L	Limit load factor
q	Dynamic pressure
R	Range
S	Wing surface
s	Spatial distance
T	Thrust force
U	Vertical gust velocity
U_σ	Limit turbulence intensity
V	Velocity
W	Weight

Subscripts

∞	Upstream
0	Design/zero-lift/sea level
1g	1g load condition
3	Begin of cruise
4	End of cruise
A	Maximum lift at maximum load point
a	Aerodynamic
b	Chosen time
c	Cruise
D	Divergence point
de	Design
e	Equivalent
ew	Empty weight
ext	External
f	Fuel
le	Leading-edge
max	Maximum
pl	Payload
s	Structural
TO	Take-off

LIST OF FIGURES

1.1	Relationship between the four main design activities.	2
3.1	Aeroelastic optimization setup steps.	8
3.2	Wing modelling examples (Werter (2017)).	9
3.3	Example of flight envelope.	10
3.4	(1-cos) gust shape idealization.(Hoblit (1988))	13
4.1	Flowchart representing the steps of this thesis work.	20
5.1	Three wings designed with the Aircraft Generator tool.	22
5.2	Sensitivities of some aircraft characteristics to input parameters for the CRM.	23
5.3	Diagram of data derivation from the inputs in the Aircraft Generation tool.	24
5.4	Diagram of aeroelastic analysis and optimization in PROTEUS (Werter & De Breuker (2016)).	26
5.5	Vertical deflection due to concentrated load on the tip comparison.	27
5.6	MAC for the aircraft structure comparison.	27
5.7	Lift distribution comparison.	28
5.8	Displacement in trim condition comparison.	29
5.9	Gust response on clamped wing comparison.	29
5.10	Gust response comparison between Free-flying (NASTRAN) and clamped wing (PROTEUS).	31
5.11	Flight envelope for the three aircraft compared.	32
5.12	Flowchart representing the outer-loop simplified structure.	33
6.1	Example of maneuver diagram. In blue the four maneuvers considered.	36
6.2	Fuel level study for an aircraft with span = 35 m and $MTOW = 75$ tons.	37
6.3	(1-cos) gust shape for different half gust lengths.	37
6.4	Convergence study for the discretization parameters.	38
6.5	Design regions of the wing.	40
6.6	Optimization cases analyzed in this research.	42
7.1	Comparison between gust sized regions and leading-edge sweep angle.	44
7.2	Comparison between structural wing weight and leading-edge seep angle.	45
7.3	Torsion distribution at different Λ_{LE} for $b = 35m$ and $MTOW = 50t$ aircraft.	45
7.4	Comparison between gust sized regions and aspect ratio ($\Lambda_{LE} = 35^\circ$).	46
7.5	Comparison between bending structural stiffness and aspect ratio.	47
7.6	Comparison of regions with strain and buckling constraints for gust loads above cut-off value of 0.6 and aspect ratio.	47

7.7	Flight envelope of $MTOW = 5t$ and $\Lambda_{LE} = 35^\circ$ aircraft configuration for three different wingspans.	48
7.8	Comparison between the percentage of gust sized regions and $MTOW$	49
7.9	Wing characteristics by changing the $MTOW$ at constant span and sweep.	49
7.10	Comparison between materials at $b = 35m$	50
7.11	Comparison between materials by changing b and $MTOW$	51
7.12	Top (left) and lower (right) wing panels in-plane stiffness.	51
7.13	Maximum root bending moment caused by gust loads compared between the three different methods of gust load inclusion.	53
7.14	Comparison between dynamic and outer-loop optimization by varying the intensity of the manoeuvre loads in regions sized by gust and normalized wing mass difference.	53
8.1	Expected percentage of wing structure sized mainly by gust loads depending by Λ_{LE} , AR and W_{TO}/b^2 of the aircraft. In red the two study cases analyzed.	56
8.2	Critical load cases for the dynamically optimized Dash 8 wing (buckling).	59
8.3	Critical load cases for the dynamically optimized Boeing 787 wing (buckling).	59
A.1	Experimental formula for Range calculation from $MTOW$	63
A.2	Wing loading empirical formula.	64
A.3	Taper ratio empirical formula.	65
A.4	Empty weight fraction versus fuel fraction (Torenbeek (2013)).	66
A.5	Number of ribs empirical formula.	67
C.1	Illustrative explanation of how the parameters are changed by keeping the other two constant in the aircraft generator tool.	74
C.2	Flight envelope of $MTOW = 50t$ and $b = 35m$ aircraft configuration for three different leading-edge sweep angles.	74
C.3	Comparison between gust sized regions and W_{TO}/b^2 ($\Lambda_{LE} = 35^\circ$).	75
C.4	Flight envelope of $\Lambda_{LE} = 35^\circ$ and $b = 35m$ aircraft configuration for two different maximum take-off weights.	75
C.5	Comparison between materials at $b = 35m$ for percentage of gust sized regions.	76
C.6	Comparison between materials by changing b and $MTOW$ for percentage of gust sized regions.	76

LIST OF TABLES

3.1	Summary of the literature reviewed divided by type of aircraft.	15
3.2	Principal aeroelastic optimization tools reviewed.	16
5.1	Validation of the aircraft generator with reference data.	25
5.2	Trim characteristics comparison.	28
6.1	Load cases (* = derived from EAS/Mach and altitude).	36
6.2	Discretization parameters used to build the aircraft model.	38
6.3	Material properties.	39
6.4	Aeroelastic optimization setup.	40
7.1	Relative time difference between different gust response inclusion methods.	53
8.1	Case studies data and comparison between predictions and results.	58
B.1	Optimization cases listed.	70
B.2	Optimization cases listed (Continuation).	71

1

INTRODUCTION

A characteristic of every design process, regardless of the type of industry to which the product belongs, is the compromise between obtaining the best performances while keeping production costs as low as possible. A popular proverb claims *Time is money*, which implies the importance of time as a variable that designers have to manage greedily in order to reduce project expenses. Keeping this in mind, it is clear that between two ways that lead to the same goal, the shorter one is preferable even if entails a minimum but insignificant variation in the final result. In the same manner, if, in an engineering design process, there is a faster way to calculate the same outcomes using less computational power, the designer would probably follow this path. However, the answers to questions like ‘which way is shorter?’ as well as ‘do both ways lead to the same place?’ are not always known a priori, especially in an engineering environment, and required for a detailed analysis to be answered.

However, owing to the constant growth of the available computational power at a very fast rate, the wing design procedure has changed substantially during the last fifty years. For this reason, performing aeroelastic optimization of the wing, which in the past were a time-demanding procedure, nowadays has become a widespread practice. Indeed, it is performed from the top to the bottom of the whole aircraft design process, whose main steps according to Torenbeek (2013) are shown in Figure 1.1. First, as the diagram show, the design requirements are established by the market demand, the customer desires and the technological improvements coming from scientific research. Then, the product design process can be divided into three main phases: the conceptual design phase, the preliminary design phase and the detailed design phase. The conceptual design phase is the first part of the project in which specific design requirements and major decisions regarding components configuration are taken. In this phase, the general geometric, performance and weight characteristics are retrieved according to empirical data, to the individual experience of the engineers and to conceptual aircraft

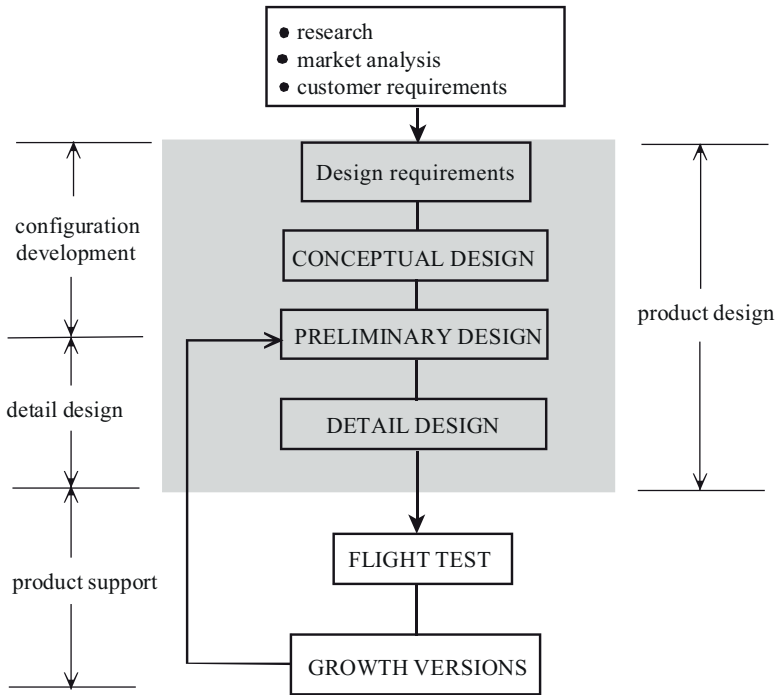


Figure 1.1: Relationship between the four main design activities.

design formulae, well explained in the aircraft design books of Roskam (1985), Sadraey (2013) and Torenbeek (2013). The purpose of this phase is to generate a competitive proposal for a feasible design that fulfills the requirements of the project. After the baseline of the aircraft is defined, the design process enters the preliminary sizing phase.

The preliminary sizing phase is the first calculation phase, during which the main features of each component and the major technical data are retrieved. The aeroelastic optimization carried out in this phase have the main goal of ensuring that the aircraft structure has enough strength and stiffness to bear the loads that an aircraft could face during possible flight missions while keeping the entire aircraft as light as possible. For this reason, selecting the best critical load cases to be included in the optimization is fundamental to achieve a reliable aircraft design. Indeed, the load cases choice is extremely determinant in what will be the final aircraft configuration and changing the loads even slightly would probably cause a modification in the entire aircraft design. When the flight conditions in which the aircraft response will be simulated are chosen, it is necessary to take into account that the addition of a load case increases the computational time of every optimization loop as well as the time required by the optimizer to find the best design that fits into the design requirements. The load cases can be divided in static ones, such as manoeuvre loads, for which the loads can be considered constant in the time domain, and dynamic ones, including gust and landing loads, which

are time-dependent. Therefore, in this case, a transient response analysis is required to simulate the aircraft behaviour. This type of analysis demands more computational time than a static simulation and, for this reason, including a dynamic load case into an aeroelastic optimization implies a huge rise in time per each optimizer iteration.

The contribution of this thesis to the aircraft design state of the art regards the load case choosing process, for which, at the moment, in research or conceptual works it is based on the personal experience of the researchers or on the results that come from the analysis of practical experiments, while for industrial works it follows certification specifications depending by the aircraft category, which indicate only the minimum amount of load cases required. However, a methodical way to choose the load cases does not exist in the literature, especially concerning the gust loads and the different way they can be included in the optimization loop. Throughout this work, the author aims to develop a systematic engineering approach that helps the structural engineer to choose if considering the gust load cases and how to include them into the aeroelastic optimization of a general civil transport aircraft. Moreover, the author aspires to give elucidations regarding the various methodology of gust modelling and the way of integrating the gust response analysis into the optimization loop.

2

PROBLEM STATEMENT

For conventional aircraft configurations, the common practice for load case choice in early stages of preliminary sizing of an aeroplane features static manoeuvre loads over dynamic ones as the most critical that the aircraft could encounter. The choice of these types of loads is based on the experience that manoeuvre loads are generally greater in magnitude than the ones provoked by the maximum gust that could be faced by the wing in flight. In this scenario, the gusts have been mainly included as an equivalent incremental static load. However, with the introduction of composite materials, high aspect ratio wings and supersonic aeroplanes, it has been recently demonstrated that dynamic loads could become more critical than the static ones (Rajpal & De Breuker (2017)) and, thus, have a moderate influence on structural characteristics of the wing. For composite aircraft, moreover, the structure designed to actively alleviate static loads worsened, on the other hand, the dynamic response of the wing. Furthermore, wind gusts have been recognized as a source of critical fatigue loads (Zhao et al. (2016)), which can lead to a wing deterioration over many missions.

For this reason, systems for passively alleviate gust loads, such as Gust Load Alleviation (GLA), have become necessary to improve the dynamic response of gust encountering and their design became common practice in the detail design phase of modern civil transport planes in the last decades (Zhao et al. (2016)). Indeed, since the incident of a B-52H bomber during a routine mission in the west of United States, in which the vertical fin broke off in flight after being invested by severe turbulence, GLA systems received a lot of attention (Dempster & Arnoldt (1969)). The contribution of Disney (1977) was fundamental in their development, where he conceived gust and manoeuvre active alleviation systems for the C-5A, leading to numerous advantages such as decreasing the wing-root bending moment, improving handling qualities, meliorating ride comfort, as well as increasing fatigue life and decreasing the aircraft gross weight. Nevertheless, as Petersson (2009) underlined *“The optimization of the dynamic response has mostly focused on active damping via the control surfaces and not on the design of the structure*

itself.". Therefore, a solution is to design the wing considering gust as dynamic loads in the preliminary sizing phase, conceiving the wing-structure itself as a passive load alleviation system. In the 1990s, Rao (1984, 1986) and Hajela (1986) began to include dynamic loads in their models, showing the advantages in gust response and final weight of the structure. More recently, aeroelastic tailoring has played a crucial role in passive gust load lightening, especially using anisotropic characteristics of composite materials.

The main problem is that the choice of including the gusts as dynamic or static loads in the preliminary design optimization is still based on the personal experience of the researcher in academia, and one the regulation prescribed in the industrial field. It is necessary to define a systematic way to decide how to include gust in the optimization process based on objective criteria, such as the main design variables of an aircraft. In this way, the inclusion of gusts as dynamic loads would be suggested only when significant benefits are expected, otherwise, they would be avoided to save computational time. With all of this in mind, the project goal can be summarized in the following statement,

with this MSc Thesis, the author aims to define design guidelines for gust inclusions in aeroelastic optimization of a general civil transport aircraft. The indices parameters of these guidelines are general design characteristics, in detail the maximum take-off weight, the wingspan and the leading edge sweep angle.

In order to achieve this final objective, several aeroelastic optimization cases among the feasible design space are going to be investigated using the in-house aeroelastic framework software PROTEUS, developed by the PhD thesis of De Breuker (2011). The gust loads will be modelled in several ways to underline the differences between static and dynamic optimization results. Moreover, a sensitivity analysis will be operated to understand the influence of each design parameter on final aeroplane characteristics and to improve the results of the optimization. Finally, a comparison among the results of these analyses will be carried out to retrieve the mentioned design guidelines.

3

LITERATURE REVIEW

In order to develop design guidelines regarding the inclusion of gust loads in an aeroelastic optimization environment, a benchmarking study about the actual state of the art of aeroelastic optimization using dynamic gust loads is necessary. Therefore, in this chapter, an overview of the state of the art of aeroelastic optimization is explored in Section 3.1, with particular attention to aeroelastic tailoring. Then, gust load modelling is described taking into account certification regulation requirements in Section 3.2. A benchmarking study regarding the optimization problems using gusts is the core of this review, illustrated in Section 3.3 with charts that summarize the main outcomes from the comparison and the available aeroelastic optimization tools. In the end, an analysis of the literature explored is provided in Section 3.4.

3.1. AEROELASTIC OPTIMIZATION: STATE OF THE ART

The state of the art of aeroelastic optimization is widely described in the MSc thesis works of Bussemaker (2018) and in the PhD dissertations of Dillinger (2015) and of Werter (2017). Every aeroelastic optimization set up is the combination of two main processes, which are the aircraft modelling and the optimization set up phases. During the airplane modelling, its structural and aerodynamic properties are represented in a discretized way to reduce the total amount of variables, simplifying the problem and reducing the computational cost. Then, the models for the aerodynamics and for the structure are coupled together to achieve the same deformations and loads. Once the aircraft modelling part is concluded, the optimization is set up. Design variables, design objectives, constraints of the optimization and load cases to be analyzed are chosen depending on the desired aeroelastic optimization approaches. Among all the possible approach, the most renowned is surely the aeroelastic tailoring approach, which will be explained in detail in this section. The steps just described are visualized in Figure 3.1 and explained in detail in Section 3.1.1 for aircraft modelling and Section 3.1.2 for load

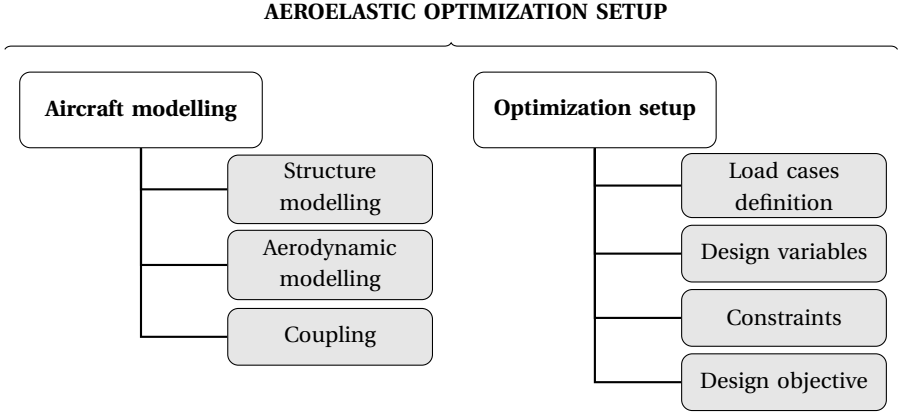


Figure 3.1: Aeroelastic optimization setup steps.

cases choice and optimization set up. These processes are important in order to build the characteristic “Aeroelastic equation”, which is evaluated by an aeroelastic analyzer for every load case in the optimization and each aeroelastic constraint. The typical form of the aeroelastic equation is (Wright & Cooper (2007)):

$$\underline{\underline{M}}_s \ddot{\underline{q}} + (\rho V \underline{\underline{C}}_a + \underline{\underline{C}}_s) \dot{\underline{q}} + (\rho V^2 \underline{\underline{K}}_a + \underline{\underline{K}}_s) \underline{q} = \underline{F}_{ext} \quad (3.1)$$

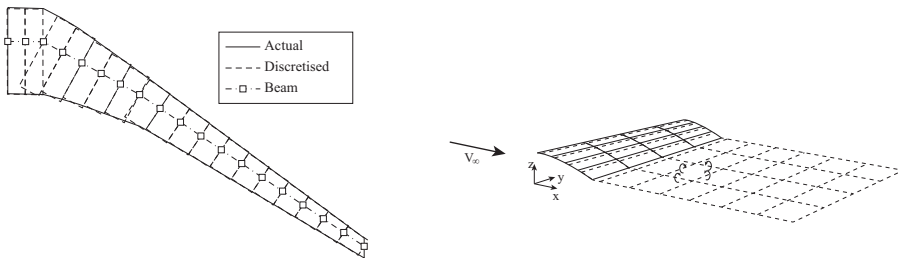
in which $\underline{\underline{M}}_s$, $\underline{\underline{C}}_s$ and $\underline{\underline{K}}_s$ are the structural mass, damping and stiffness matrices respectively, $\underline{\underline{C}}_a$ and $\underline{\underline{K}}_a$ are the aerodynamic damping and stiffness matrices, \underline{q} is the vector of generalized coordinates, typically modal coordinates, and \underline{F}_{ext} is the vector of external forces.

3.1.1. AIRCRAFT MODELLING

The first step in every aeroelastic modelling is the discretization of the structure using the Finite Element Method (FEM). In this way, the essential parts of the aeroplane are decomposed in a certain number of elements that depends on the desired accuracy and the computational power availability. The structure of an aircraft is typically composed of several different elements: shear webs, spars, skin panels, ribs and stringers. All of these components could be modelled in order to obtain an accurate representation of the structural behaviour. The most common finite elements used to represent the aeroplane structure are the shell and beam ones. Therefore, the complexity of the structure is simplified using systems like the cross-sectional modeller. An example of the cross-sectional modeller is deeply illustrated in the PhD dissertation of Werter (2017), which represent the wing with just a beam element converting the properties of each structural elements to cross-sectional properties of the beam, changing only in the span-wise direction. Afterwards, non-structural masses, fuel loads and engines are usually reported on the structure through concentrated masses since the mass model of an aircraft is significant to obtain high reliability of the optimization results (Dillinger (2015)). From the structural model, structural mass and stiffness matrices (respectively $\underline{\underline{M}}_s$ and $\underline{\underline{K}}_s$)

are computed by a structural analysis program. An example of a structural modelling is given in Figure 3.2a (Werter (2017)), in which the model is superimposed on the actual wing shape.

Secondly, the aerodynamics need to be discretized in a mesh which usually has different characteristics than the structural one. The skin of the aircraft is divided into panels in which the aerodynamic properties are computed. There are several ways to calculate the aerodynamic forces acting on a wing. However, the three most used according to Werter (2017) are the strip theory, the Doublet Lattice Method (DLM) and the Unsteady Vortex Lattice method (UVLM). The first one, also known as two-dimensional unsteady airfoil theory, adapts solutions in a closed-form on numerous specific cases. (Patil et al. (2001), Su & Cesnik (2011)). The other two methods are both based on potential flow theory, but they have different potential flow elements to represent the lifting surface. The DLM, introduced by Albano & Hodden (1969), uses doublets as the name suggests. It is the most used method for unsteady loads analysis of an aircraft. The main advantage is that accounts for the compressibility in its calculations. It is used in the famous commercial structural analyzer MSC NASTRAN (MSC Software Corporation (2004)). Finally, the UVLM solves the potential flow equations throughout a distribution of vortex rings all over the wing surfaces and on the wake. This method is implemented in the software that is going to be used, PROTEUS (Werter & De Breuker (2016)), as it allows direct calculation in the time domain and allows for free wake modelling and, thus, computation of flow around the wing. An example of wing discretization using vortex wing elements is given in Figure 3.2b (Werter (2017)). Along with the aerodynamic calculations, the aerodynamic influence coefficients (AICs) are also derived. They determine the reciprocal influence among the panels and the correlation between local down-washes and pressures (Dillinger (2015)). All of these methods are efficient and fast compared to Computational Fluid Dynamics (CFD) ones. However, some drawbacks rise from the fact that several aerodynamic phenomena are neglected. For example, DLM and UVLM, which



(a) Discretized wingbox geometry compared to the actual one.

(b) Aerodynamic discretization by vortex ring elements (dashed lines).

Figure 3.2: Wing modelling examples (Werter (2017)).

are linear panel methods, do not compute viscous drag, nonlinear compressibility effects, boundary layers and flow separation points (Katz & Plotkin (1991)). Furthermore, these methods need the introduction of down-washes on the panels to correct for the impossibility of including twist and camber into the properties of the panel. Moreover, they are limited by being reliable only at subsonic speeds. In the last years, CFD methods are gaining popularity due to their accuracy and to the availability of high-performance computers, which increase the capabilities of simulation, flight envelope coverage and physical complexity of the model, leading to a large reduction in standard wind tunnel testing (Chaput (2015)). However, during an optimization in which the performances are calculated several times, these methods are still too computationally expensive to be implemented.

After both the structural and aerodynamic properties of the aeroplane have been modelled, the two meshes are coupled. Among a variety of different methods, the most used is spline coupling which is a 3D interpolation approach that allows the link between mode shapes and aerodynamic forces (Dillinger (2015)). Generally, the modelling part terminates here, even if the model of the aircraft could be extended by defining other parts. For instance, the control system, the fuel and the engine pylon model could be added as in the wing sizing of Voss & Klimmek (2016). However, in this project, further models are neglected for reducing the computational cost of the optimization.

3.1.2. LOAD CASES CHOICE AND OPTIMIZATION SET UP

After the modelling part, load cases must be defined. The choice of the load cases is driven by different factors, among which the ones specified by the regulation entities like the European Union Aviation Safety Agency (EASA) or the Federal Aviation Administration (FAA) have to be considered. For certification of a commercial aircraft, CS-25 by EASA (2018) is the regulation reference for load specification. According to the regulatory authorities, enough points of the “flight envelope” should be chosen, considering

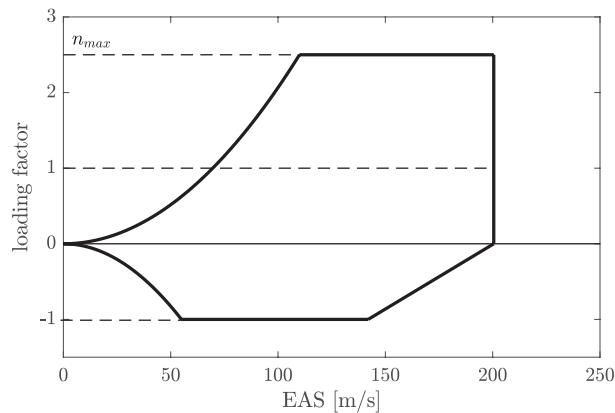


Figure 3.3: Example of flight envelope.

for each condition the critical altitudes, weights, distribution of disposable loads and compressibility effects. The flight envelope is built calculating characteristic velocities and load factors for the aircraft according to EASA (2018). An example of a flight envelope is shown in Figure 3.3, in which n indicates the load factor that is the ratio among lift produced during a certain manoeuvre and aircraft weight, and EAS indicates the Equivalent Air Speed of the aircraft at sea level. The thick line is the envelope and includes all the feasible manoeuvres that the aircraft can perform. The acceptable means of compliance indicates symmetric pitching condition and gust loads as critical for certification. The total amount of load cases is variable. For example, four cases are generally sufficient at conceptual design level like in the work of Werter (2017), while these can increase to 120 at the detailed design phase such as in the work of Handojo et al. (2018), and can rise to thousands at the certification design phase. A good example of determination algorithm of critical loads for structural optimization is given by Leitner et al. (2016). The convention is to treat all the loads as static due to the fact that dynamic ones are more expensive to be computed and, usually, static manoeuvre loads are more critical than gusts (Rajpal & De Breuker (2017)). However, this is not always true and the situation can be inverted when using composite materials. In these cases, enough quantity of gust load cases should be considered in the load envelope.

Once the disciplines are modelled and the load cases are defined, the numerical optimization framework can be set up. It is composed of the objective function, which is the aim of the minimization research, the design vector, which contains the design variables of the problem, the boundary values for these variables, and the equality and inequality constraints, which delimit the exploration field. The choice of the design variables and the objective depends on the desired optimization approach. In a general aeroelastic optimization approach, the weight minimization is the goal reached by sizing structural elements. However, the most important and efficient approach to optimize the aeroelastic response and the weight of an aircraft is the “Aeroelastic Tailoring” approach. The definition of this method was given by Shirk et al. (1986) as *“the embodiment of directional stiffness into an aircraft structural design to control aeroelastic deformation, static or dynamic, in such a fashion as to affect the aerodynamic and structural performance of that aircraft in a beneficial way.”* This approach was initially introduced by Munk (1949) in a patent that proposed a propeller design that uses anisotropic properties of wood to tailor the aeroelastic deformation of the blade. Including aeroelastic tailoring in the conceptual design of the wing leads to several advantages, including a reduction in manoeuvre drag, divergence and flutter prevention, load alleviation, favourable lift distribution, an advantageous centre of pressure position and control effectiveness improvement (Weisshaar (1981), Werter (2017)). Therefore, aeroelastic tailoring can be considered as a “passive load alleviation” system (Handojo et al. (2018)), which gives the structure the ability to reduce determined loads and uncouple bending and torsion arising from external solicitations. Furthermore, as explained by Harmin et al. (2011) and Werter (2017), it became particularly relevant with the introduction of composite materials, which are intrinsically anisotropic and therefore capable of different stiffness properties in different directions. Composites are efficient for improving bend-twist coupling and the lightness of the structure thanks to their superior strength to weight ratio. More-

over, they have high fatigue and damage tolerance. An example of a complete process of aeroelastic tailoring from the conceptual design to the manufacturing of the wing is given by Meddaikar et al. (2018). For more information about tailoring techniques, the reader is referred to the excellent overview of the topic written by Jutte & Stanford (2014).

3.2. GUST MODELLING

A gust is a strong and sudden rush of wind which provokes an increase in the angle of attack and, thus, the lift force acting on the wing. Therefore, gusts are intrinsically complex, random and dynamic phenomena that are critical for sizing the wing but difficult to model. Moreover, an accurate dynamic response calculation of an aircraft subjected to a gust is computationally demanding. The earliest studies of an aircraft encountering a gust were performed by Pratt (1953) and Bisplinghoff et al. (1955) with one of the earliest contributors being Küssner (Rao (1984)). Since then, the gusts have been modelled in many ways, among which four have been accepted during the years from regulating authorities as acceptable means of compliance for aircraft certification. These models are the Pratt formula, the probabilistic load factor, the (1-cos) discrete gust and, finally, the continuous random turbulence.

Even if gusts are essentially dynamic as stated before, they have been approximated as static loads to reduce the computational time of the optimization process. The most common static representation is given by the Pratt formula, seen below:

$$\Delta n_{max} = \frac{\Delta L}{W} = K_g \frac{U_{de} V_e \rho_0 C_{L\alpha}}{2(W/S)} \quad (3.2)$$

Introduced by Pratt (1953), this equation calculates the increment in lift caused by a step gust as a loading factor increment function of the gust equivalent vertical speed U_{de} , the aircraft equivalent speed V_e , the wing surface S , the wing lift-slope coefficient $C_{L\alpha}$ and the airplane weight W . The equivalent gust speed is correlated to the actual speed by the density ratio ($U_{de} = U_0 \sqrt{\rho/\rho_0}$). An alleviation factor K_g is introduced depending on the aircraft controls performances:

$$K_g = \frac{0.88\mu_g}{5.3 + \mu_g} \quad \mu_g = \frac{2(W/S)}{\rho g c C_{L\alpha}} \quad (3.3)$$

This formula, which was included in FAR 25 regulation (Code of Federal Regulations No. 14 (1988)), works properly in the conceptual design phase. It is a reasonable method to be used with a very low computational effort to attain a first estimation of the gust loads acting on a wing (Voss & Klimmek (2016)). Another static method included in FAR 25 was used by Yang et al. (1988) and Yang & Nikolaidis (1991). It is based on the fact that gust is a random turbulent disturbance with an amplitude that is large compared to the wingspan (Code of Federal Regulations No. 14 (1988)). Therefore, a suitable way to model the maximum gust loading is the probability distribution of gust encountering in a fixed period. It is described by Yang et al. (1988) according to the FAR 25 regulation. The formulas are not provided here because this method has shown sparse applications.

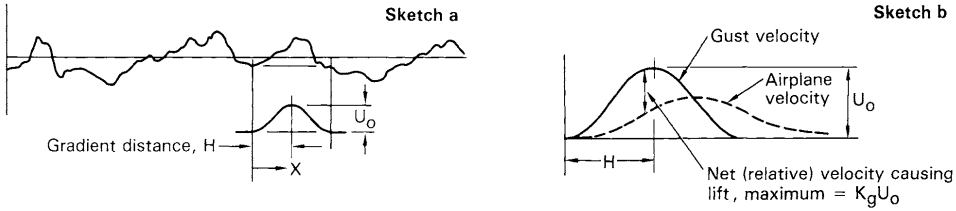


Figure 3.4: (1-cos) gust shape idealization.(Hoblit (1988))

The current regulation for aircraft certification (CS-25, EASA (2018)) defines gusts as a dynamic load through two methodologies: (1-cos) discrete gust and continuous turbulence design criteria. The first method assumes that the aeroplane encounters a symmetrical individual vertical gust, or “discrete gust”, idealizing the structure of the gust with a pulse whose shape follows the equation:

$$U = \frac{1}{2} U_0 \left[1 - \cos\left(\frac{\pi s}{H}\right) \right] \quad (3.4)$$

in which U is the gust velocity, U_0 is the design gust velocity in equivalent airspeed depending on altitude and aircraft weight as specified in the documentation (CS.341, EASA (2018)), s is the distance penetrated in the gust and H is the gust gradient, which is the distance needed by the gust to reach the maximum value ($9m < H < 107m$). A sufficient number of gust gradients should be included in the analysis. For the characteristic shape, this model prescribed by EASA is often called the (1-cos) discrete gust model, which is an idealization of the more complex shapes that form the atmospheric turbulence as can be appreciated in Figure 3.4 (Hoblit (1988)). As can be observed, also the aircraft response assumes the (1-cos) shape but with a certain phase delay and a certain amount of damping. It is discretized in the time domain to be easily managed by structural analyzers. Since several gust cases should be calculated, often only the worst gusts are predicted and analyzed. Good examples of efficient prediction of worst (1-cos) gust loads are given by Khodparast et al. (2012) and Knoblach (2013). The last method considers the gust environment as continuous random turbulence that can be seen as a summation of individual gusts with simple geometrical shapes and intensities. A power spectral distribution of the gust velocity in frequency domain captures this mix of shapes. EASA (2018) indicates the Von Karman power spectral distribution as the most applied one to represent the atmospheric turbulence. The limit load P_L is calculated for all critical altitudes, speeds, weight conditions and fuel distributions with the following formula:

$$P_L = P_{L_{1g}} \pm U_\sigma \bar{A} \quad (3.5)$$

in which $P_{L_{1g}}$ is the steady 1g load for the condition, U_σ is the limit turbulence intensity as True Air Speed (TAS) and \bar{A} is the ratio of root mean square of the incremental load to root mean square of velocity. \bar{A} depends on the spectral distribution and on the frequency response function that relates loads on aircraft structure to the turbulence

calculated with dynamic analysis as explained in EASA (2018). A good description of this method is also given by Stauffer & Hoblit (1973).

3.3. WING OPTIMIZATION USING GUST LOADS

A benchmarking of the current methodologies of designing a wing including gust loads is presented here. Since gust loads are dynamic phenomena, they require a time-dependent analysis that is computationally more expensive than a static one. Furthermore, the number of simulations has to be high in order to include enough gust lengths since the critical load cases are not known a priori, resulting in a computational inefficient procedure (Rajpal & De Breuker (2017)). Therefore, historically, the tendency was to avoid their inclusion and, when included, they were considered using the static approximation formula presented by Pratt (1953). However, as Petersson (2009) states, gust loads together with flutter and control effectiveness are important for sizing the aircraft for static and fatigue strength, critical for light or high aspect ratio wings (Yu et al. (2017)) and very demanding requirements for certification of commercial transport aircraft (Vio & Cooper (2008)). Moreover, gusts can affect different aspects of aircrafts' operations like flight stability and safety (Su & Cesnik (2011)). In these cases, the dynamic representation of the gust is essential to give satisfactory predictions. The interest in performing wing optimization using gust loads was concentrated in two decades. The first period took place over the 1990s, during which the interest in this topic arose for those who performed system reliability approaches and for those who wanted to investigate the gust response of a wing. The second one began with the implementation of composite material in the aeronautical field and lasts until today, in which the number of literature available is increasing.

The first studies about optimization of the wings including dynamic loads were done during the 1980s by S. S. Rao and P. Hajela. Indeed, Rao (1984, 1986) performed an optimization of the structure of wing considering a discrete (1-cos) type. Previously, only studies on the aeroelastic response of an aircraft that encountered a gust were carried out, where Küssner was the earliest contributor (Bisplinghoff et al. (1955)). The importance of including dynamic loads calculation, according to Rao (1984), was due to the fact that aircraft were becoming faster and larger. A faster speed of flight means thinner airfoils, a more slender body and more dynamic pressure while a larger span means higher lift slope, both aspects that emphasize the gust induced stresses (Rao (1986)). At the same time, a growth of interest in wing design subjected to gusts was registered in a system reliability approach scenario, in which the main authors were Yang et al. (1988) and Yang & Nikolaidis (1991). The reason why the interest in gusts has begun in the system reliability field is that the purpose of this approach is to design a structure that can bear any possible failure causes, among which gusts are significant ones. This method takes into account the redundancy of the structural elements returning a safety measure for the whole structure seen as a system. Since the system reliability calculation is quite expensive, the dynamic effects were neglected and the gusts were treated as static loads.

Table 3.1: Summary of the literature reviewed divided by type of aircraft.

Aircraft type	Composite Material	Literature reviewed	Total comp.	Total metal.	Tot.
Civil transport	-	Hajela (1986), Hajela & Bach (1989), D'Vari & Baker (1993)	-	3	9
	Yes	Werter & De Breuker (2015), Petersson (2009), Schuhmacher et al. (2012), Werter (2017), Rajpal & De Breuker (2017), Handojo et al. (2018)	6	-	
Fighter	-	Pettit & Grandhi (2003)	-	1	1
Flying wing	Yes	Voss & Klimmek (2016), Yu et al. (2017), Vio & Cooper (2008)	3	-	3
Supersonic transport	-	Rao (1984, 1986), D'Vari & Baker (1993)	-	3	3
High span straight wing	-	Yang et al. (1988), Yang & Nikolaidis (1991)	-	2	6
	Yes	Petersson & Daoud (2012), Kim & Hwang (2005), Schuhmacher et al. (2012), Werter & De Breuker (2015)	4	-	
			13	9	22

With the introduction of composite materials in the aircraft industry in the last decade, the dynamic loads were considered again as they can become more critical than the static ones (Rajpal & De Breuker (2017)). Therefore, it raises the necessity to include gust loads in the preliminary design of composite wings, for which the directional stiffness of the material can be used to counteract adverse responses while the structure can be lightened thanks to its high specific stiffness and strength (Werter (2017)). A detailed explanation about composites properties and lamination theory could be found in the PhD dissertation of Dillinger (2015). Regarding aeroelastic tailoring approach for dynamic gust response, a lot of research has been carried out at the Delft University of Technology in collaboration with DLR, the German Aerospace Research Institute. Among these, important works for the author's thesis project are the works of Werter & De Breuker (2015), Werter (2017), Rajpal & De Breuker (2017) and Handojo et al. (2018).

In Table 3.1, a summary of the literature reviewed is reported. It is divided by type of aircraft on which wing design using gust loads was performed. Among the 22 air-

Table 3.2: Principal aeroelastic optimization tools reviewed.

Software	Sensitivities to gust response	Dynamic gust models	Applicability
PROTEUS (Werter & De Breuker (2016))	Yes	(1-cos) discrete	Academic research at TU Delft
ASTROS (Neill & Herdeen (1997))	No	(1-cos) discrete, continuous turbulence	Academic research, preliminary sizing
MSC NASTRAN (MSC Software Corporation (2004))	No	(1-cos) discrete, continuous turbulence	Academic research, detail design, industrial design
ACO-AMO (Grihon (2018), Iorga et al. (2016))	No	(1-cos) discrete, continuous turbulence	AIRBUS detail design, industrial design
LAGRANGE (Zotemantel (1993))	Yes	(1-cos) discrete	Academic research (born as AIRBUS industrial tool)

craft optimization studies that have been reviewed, there is a trend of choosing large civil transport aircraft (9 times) and high span straight wing ones (6 times). Moreover, it can be noticed that in the last decade (2008-2018) composite aircraft are chosen more often for passive gust alleviation. The commonly used programs for aeroelastic optimization found in this literature review are illustrated in Table 3.2, in which the software is presented along with the literature in which they are illustrated, their applicability and the dynamic gust models they offer. Furthermore, an investigation on the type of sensitivities available in each optimizer has been carried out, focusing on the possibility of having sensitivities on the dynamic gust response and, thus, verifying if the aircraft can be optimized for passive gust loads alleviation. As could be noticed, only PROTEUS and LAGRANGE have this characteristic, necessary for the type of optimization required in this thesis.

3.4. ANALYSIS

As a result of this literature review, it can be claimed that not many studies have been performed in the field of gust dynamic response inclusion in the aeroelastic optimization. Indeed, during the research, many examples of optimization including gust only as an incremental factor have been found. Nevertheless, the purpose of this literature research is to give an overview of how aeroelastic optimization including dynamic gust

response analysis has been performed. Therefore, many of the findings were neglected leaving a total amount of 22 aircraft design to be compared. The literature confirmed the necessity of including gust loads as dynamic loads in aeroelastic optimization as hypothesized by the author of the thesis. The main reason is that this type of load could become critical in aircraft made by composite materials, in very light structures or high aspect ratio wing aircraft. It has been reported that including a dynamic gust response in the structural sizing of a wing could lead to passive gust load alleviation, resulting in beneficial lightening of the structure. To reach this purpose, aeroelastic tailoring is a powerful optimization approach that can lead to improvements of the gust response as well as reducing the coupling between bending and twisting deformation of the wing. Thus, the importance of the author's MSc thesis work in defining design guidelines for gust load inclusion in aircraft aeroelastic optimization is clear, as the importance to understand when these benefits are foreseeable and when, on the other hand, the inclusion just lead to an increment of computational cost.

Following the benchmarking study, PROTEUS has been chosen as aeroelastic optimization program. The main reason for this choice is its ability to easily include a dynamic response in its optimization loop, which is not possible in the more famous commercial tool MSC NASTRAN. Another reason is its ability to manage lamination parameters for aeroelastic tailoring. Moreover, following this review, the general commercial transport aircraft has been chosen as the aircraft category for this thesis investigation as a result of the high number of applications found. The composite configuration will be explored as well as the metallic one. Finally, the loadcases will be limited to a few symmetric pull-up and push-down manoeuvres and a few gust load cases since this is the common practice at a preliminary design level.

4

METHODOLOGY

The main hypothesis that has to be confirmed throughout this thesis work is the existence of a correlation between general characteristics of the aircraft and the influence of gust loads on the structural sizing of the wing. To demonstrate this claim, various designs will be performed covering the feasible design space generated by three major design parameters. The chosen aeroelastic analyzer and optimizer is the in-house developed software, PROTEUS. Since aeroelastic optimization is computationally expensive, a high-performance computer of the faculty has been used to run several optimization cases. Afterwards, the results of this optimization cycles is compared with many designs obtained using different gust modelling methods, different types of material and with optimizations lacking the gust load case. In Figure 4.1, the path followed to achieve the goals of this thesis is presented as a flow chart. In the following paragraph, the process is described step by step.

First, the functionalities of the in-house software PROTEUS need to be validated through a comparison with the commercial solver MSC NASTRAN. In addition, a conceptual design tool is built to create PROTEUS input files. This tool generates aircraft properties from three general aircraft parameters that are discussed in the next chapter. Once this tool has been validated, the optimization is set up, defining modelling parameters and load case specifics. Preliminary studies such as convergence tests or fuel analyses are carried to understand the number of finite elements and the critical fuel level respectively. Several optimization loops are then computed. They can be divided into two cycles. The objective of the first one is exploring the design space, while the second aims to achieve a sufficient number of results. In this phase, the type of material, the gust model, the method of gust response inclusion into the optimization are added as variables of the analysis. Finally, after a detailed examination of the results, the design guidelines are retrieved. To show their efficacy, some case studies are analyzed and compared with expected results from the guidelines are applied are presented.

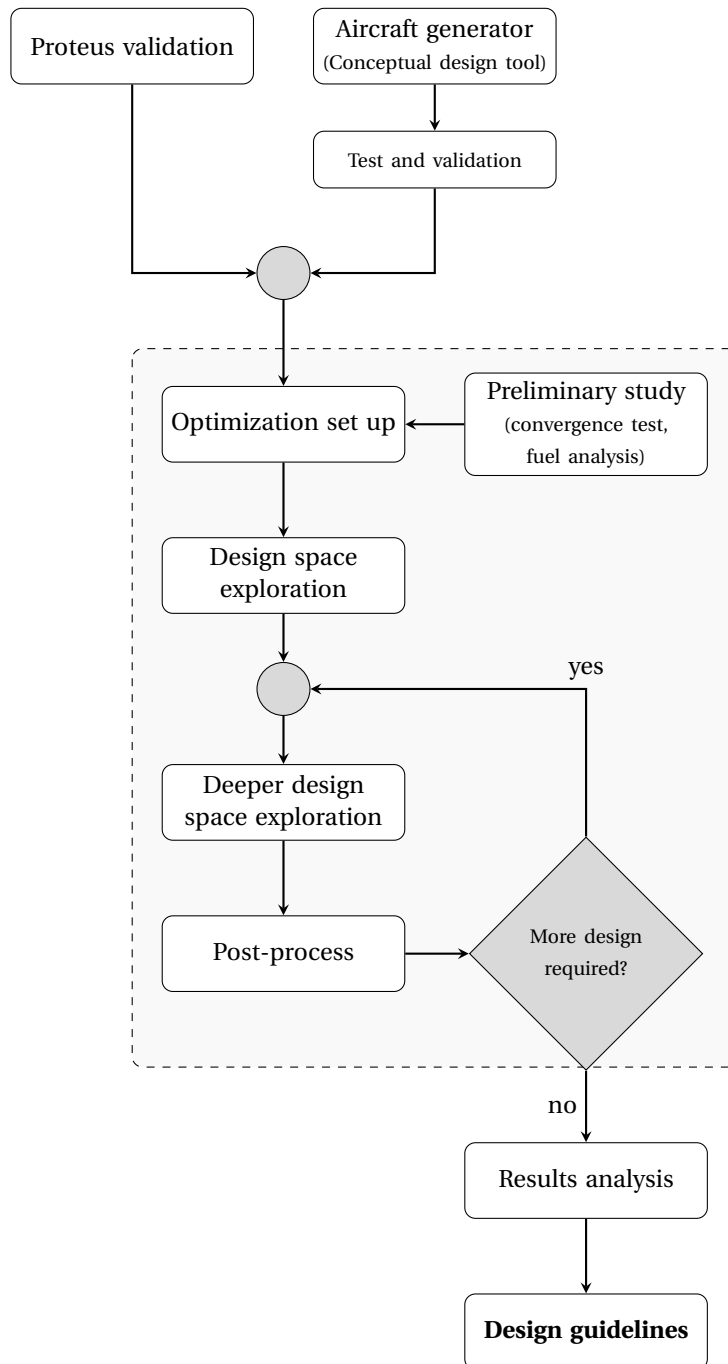


Figure 4.1: Flowchart representing the steps of this thesis work.

5

OPTIMIZATION FRAMEWORK

The optimization framework is composed of two parts: a pre-processor which generates the aircraft input files required for the optimization, and the optimizer, which is the in-house software PROTEUS. The aircraft generator and its validation are presented in Section 5.1 while the aeroelastic framework PROTEUS is reported in Section 5.2 along with its comparison with the commercial software MSC NASTRAN. Moreover, an outer-loop for the gust analysis has been built in PROTEUS to verify the effects of excluding the gust response calculation from the optimization loop. This way, the analysis is carried out externally and gust loads are imported just as Equivalent Static Load (ESL). The optimizer is therefore lacking sensitivities to the dynamic gust response. This functionality, which is common practice in the industrial environment, is shown in Section 5.3, along with the way it has been built.

5.1. PRE-PROCESSOR: AIRCRAFT GENERATOR TOOL

The research of the design guidelines demands the computation of several optimization cases to explore the design space of civil jet aircraft category. Therefore, this conceptual design tool is fundamental for rapidly generating the aircraft main parameters, which are the starting point of the aeroelastic optimization. The aircraft generation is carried out from three general design variables, which are the Maximum Take-Off Weight ($MTOW$), the wingspan (b) and the leading-edge sweep angle (Λ_{LE}). These three parameters will be used as indicators in the design guidelines resulting from this thesis. Their choice is based on the following criteria:

- Relevance from the perspective of the structural engineer;
- Ability to describe a large range of different civil aircraft;
- Capability of defining uniquely a specific design;

- Reducing the total number of parameters as much as possible;
- Ability to represent principal aircraft characteristics;
- Direct correlation to top-level requirements (TLRs) of the aircraft design.

Some results of this conceptual design tool are shown for three illustrative input triplets in Figure 5.1, in which the wing shape, the spars, the main landing gear (MLG) and engine position are featured. It is important to describe the main effects that each parameter has on the wing characteristics. The *MTOW* is the main influencing parameter for the wing area, while the wingspan defines the distance of the wingtip to the fuselage. Therefore, when the span is constant, Λ_{LE} changes the effective beam length. On the other hand, when *MTOW* and Λ_{LE} are fixed, the wingspan is responsible for changing the aspect ratio (*AR*) of the wing, keeping the wing leading-edge unaltered. The leading-edge sweep angle is directly correlated to the cruise speed of the aircraft, which alters the dynamic pressure and, thus, the aeroelastic effects on the wings. To have a better understanding the correlation between design inputs and general aeroplane characteristics, the author has calculated the sensitivities for the NASA CRM, which are showed in Figure 5.2. A blue square indicates a positive sensitivity of the parameter to the design variable, a white one a neutral dependency and a red one an inverted correlation, for which the growth of the input implies a reduction of the related characteristic.

The program is written in MS EXCEL for simplicity since the input file of PROTEUS is in the same format. The approach used to write the program is a combination of con-

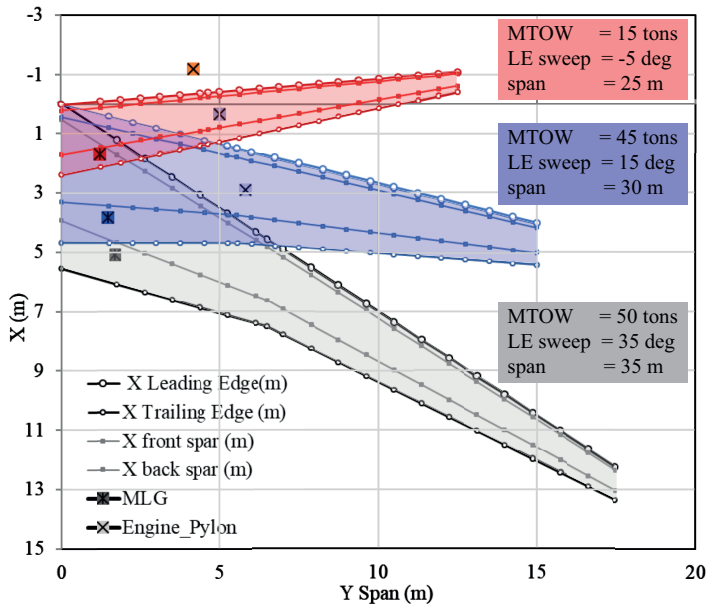


Figure 5.1: Three wings designed with the Aircraft Generator tool.

	M_{cruise}	V_{max}	Range	W/S	$(L/D)_{max}$	CL	T_{max}/W	AR	S	W_{ew}	W_f	W_{pl}
Λ_{LE}	Blue	Blue				Red	Light Blue			Light Red		Blue
MTOW			Blue		Light Red			Red	Light Blue	Blue	Light Blue	Red
span				Light Blue	Blue	Light Blue	Red	Blue	Light Red	Red		Blue

Figure 5.2: Sensitivities of some aircraft characteristics to input parameters for the CRM.

ceptual design and preliminary sizing formula (Roskam (1985), Raymer (1992), Sadraey (2013), Torenbeek (2013)), also considering empirical formulae retrieved from data collection of several civil aircraft and experimental data attained by Airbus and Boeing aircraft families (Jenkinson et al. (2001)). The general structure of the tool is presented in Figure 5.3. As previously explained, the starting points of the program are three input variables, which are $MTOW$, leading-edge sweep angle and wingspan. Once the designer inserts these input parameters, the top-level requirements, such as range or stall speed, are calculated using empirical formulae derived from the linear interpolation the characteristics of about thirty civil aircraft. Once the TLRs are derived, general performances coefficients are derived using formulae and typical aeronautical values. To execute this calculation, some constants are introduced. The maximum lift coefficient (CL_{max}), the Specific Fuel Consumption (SFC) and the flight altitude (h) are considered constant among all the aircraft of the same category. An important value obtained here is the maximum wing loading $(W/S)_{max}$, which is derived empirically with good approximation, as will be shown later in the validation of the tool. From this data and the wingspan it is possible to derive wing shape information such as wing surface (S), mean aerodynamic chord (mac) and aspect ratio (AR). At the same time, the principal weights of the aircraft are retrieved using Class I estimation (Sadraey (2013)). Indeed, the fuel weight (W_f) can be calculated from the range while the weight of the empty aircraft (W_{ew}) is recovered from the fuel weight employing a graphical formula introduced by Torenbeek (2013). Then the payload (W_{pl}) can be easily determined by inverting the unity equation, which is:

$$\frac{W_{ew}}{W_{to}} + \frac{W_f}{W_{to}} + \frac{W_{pl}}{W_{to}} = 1 \quad (5.1)$$

in which W_{to} is the $MTOW$. Once all of the main features of the plane are calculated, the load cases and the aircraft characteristics are determined. As better explained in the next chapter, the five load cases are two pull-up manoeuvres, two push-down ones and one gust load case with several gust lengths. The load cases are dependent by each aircraft design. The manoeuvring speed, the gust encountering angle and the pull-up manoeuvres load factor intensity are the load case variables. The aircraft characteristics, finally, individuates the fuselage sizes, the mass distribution and the wing specifications in detail. The Common Research Model (CRM) of NASA is used as a reference for the mass distribution of the aeroplane. In creating this tool, some approximations were im-

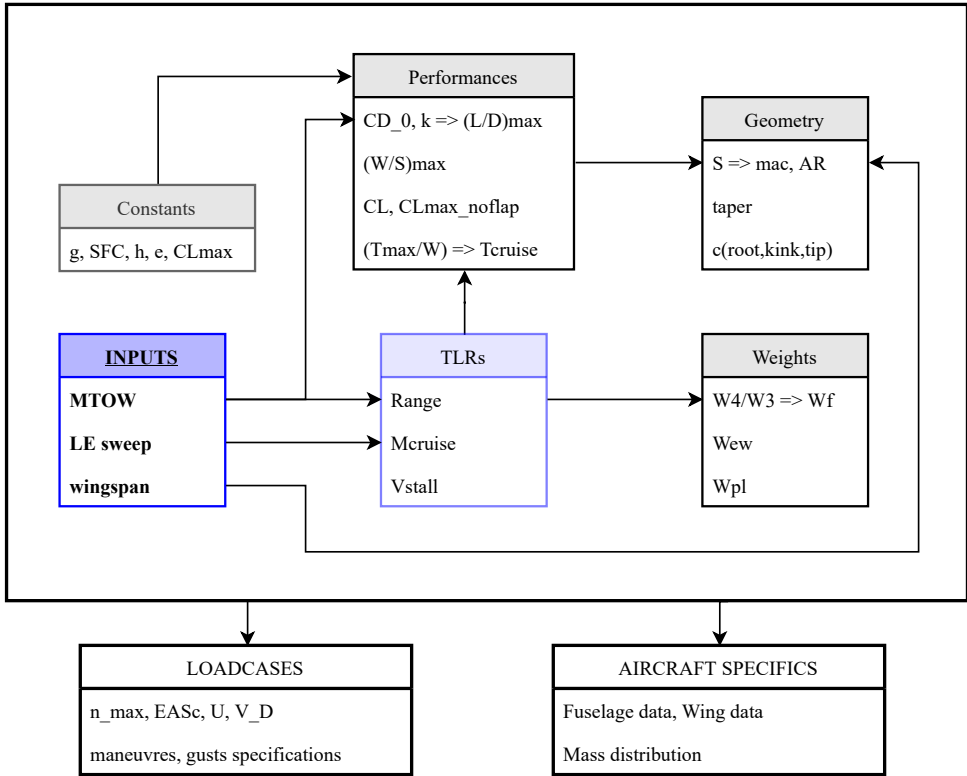


Figure 5.3: Diagram of data derivation from the inputs in the Aircraft Generation tool.

plemented, including considering the same twist and airfoil distribution along the wing for different designs. However, this approximation is reasonable since their computation requires a long dedicated analysis, which is not within the scope of this tool. For a detailed list of all the main formulae used for the calculation as well as the studies used for deriving the empirical ones, the reader is referred to Appendix A.

In Table 5.1, the comparison between the results of this tool and the actual data of several aeroplanes is given as validation of the program. The percentages represent the relative errors of the value calculated with the generator with respect to the actual ones. The table shows great consistency between the model and the actual data, with excellent equivalence in geometrical (S , mac and AR) and top-level requirements (M_{cruise} , range and W/S) data, which are fundamental for generating a realistic design. The majority of the errors are located in the weight division, particularly in the payload. A closer look reveals that also unique designs such as the enormous A380-800 generate differences. However, the aim of this tool is not to replicate the existing design exactly, but to generate feasible designs to be inputs for the optimization carried on in PROTEUS. Therefore, considering the relatively small errors, the program is demonstrated to be effective.

Table 5.1: Validation of the aircraft generator with reference data.

	E145	A220	B737	A320	B767	A350	B777	B747	A380
SweepLE	26	27.5	28	28	34	35	34.6	37.5	36.5
MTOW (kg)	19200	63050	69400	78000	181437	280000	286897	396830	575000
Span (m)	20.04	35.1	34.3	35.8	47.57	64.75	60.9	62.3	79.75
Mcruise	2.46%	0.90%	1.02%	0.38%	1.31%	1.91%	1.13%	0.11%	0.48%
Vmax (m/s)	4.15%	3.74%	3.69%	4.29%	2.50%	2.60%	2.74%	3.75%	4.65%
Range (km)	2.52%	10.88%	6.87%	2.02%	4.86%	2.49%	7.36%	4.34%	0.11%
W/S (N/m ²)	0.49%	1.40%	4.07%	2.22%	1.38%	3.85%	1.81%	10.97%	0.47%
S (m ²)	0.49%	1.42%	3.92%	2.27%	1.36%	3.71%	1.84%	13.14%	0.47%
mac (m)	0.49%	1.39%	3.92%	2.20%	1.36%	3.71%	1.84%	13.14%	0.46%
AR	0.53%	1.46%	4.13%	1.84%	1.35%	3.80%	1.93%	11.58%	0.42%
Wew	0.85%	3.53%	5.00%	3.21%	1.93%	5.71%	7.76%	7.84%	7.51%
Wf	13.63%	0.64%	22.69%	12.85%	8.83%	4.04%	5.48%	4.55%	1.23%
Wpl	6.15%	8.76%	21.23%	8.28%	38.97%	9.28%	12.61%	15.90%	47.46%
engine	13.49%	11.95%	12.47%	8.64%	29.18%	5.88%	6.17%	8.63%	18.01%

5.2. AEROELASTIC FRAMEWORK: PROTEUS

PROTEUS is the Delft University of Technology in-house aeroelastic framework for aeroelastic aircraft optimization and tailoring, developed in a MATLAB environment. Initialized by De Breuker (2011), it was used and developed by several students at the university through several research works, including Werter & De Breuker (2015), Werter (2017), Rajpal & De Breuker (2017) and Meddaikar et al. (2018). A good explanation of the structure of this tool is given in the work by Werter & De Breuker (2016), the theoretical knowledge on which the program is based is given by Werter (2017) whereas the static aeroelastic analyzer is explained by De Breuker et al. (2011). The objective of this framework is to improve the conceptual design of aircraft wings by sizing the structural elements and by including aeroelasticity. Due to the fact that an aeroelastic environment is quite computationally expensive, the three-dimensional structure is split into several sections for which cross-sectional properties of equivalent linear beam elements are computed. For the aerodynamics, a linear model is built using potential flow theory through unsteady vortex lattice method. The structure of the program is composed mainly of four modules:

- **Input part**, in which geometry and load cases are inserted,
- **Analysis**, in which separately nonlinear static and linear dynamic aeroelastic calculations are performed,
- **Optimization**, the core of the program, consisting of the optimizer,
- **Post-processing**, composed by the cross-sectional modeller.

A schematic representation of the aeroelastic analysis and optimization loop is represented in Figure 5.4 by Werter & De Breuker (2016). The program is preferred to the popular commercial finite element based analysis software MSC NASTRAN due to its ability

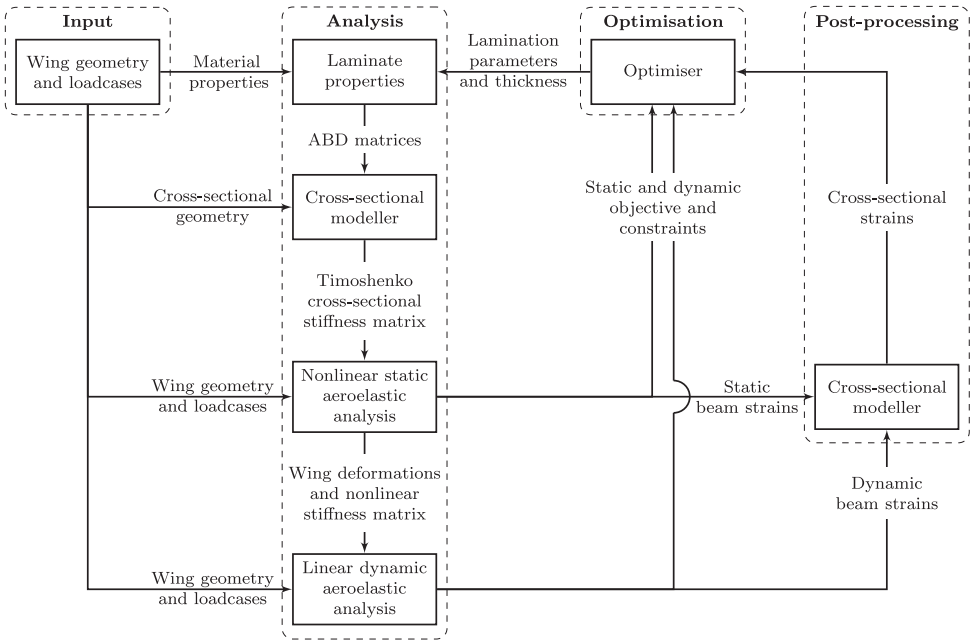


Figure 5.4: Diagram of aeroelastic analysis and optimization in PROTEUS (Werter & De Breuker (2016)).

to execute optimization including dynamic discrete (1-cos) gust response and sensitivity analyses. However, the main drawback of PROTEUS is that the wing is clamped for dynamic analyses, which means that the wing root is constrained in all the directions. To have a better understanding of the differences between MSC NASTRAN and PROTEUS and to validate the available analyses of the in-house tool, a comparison of the two programs is here proposed.

The comparison between PROTEUS and MSC NASTRAN is divided into four different analyses: concentrated force in the wingtip static deformation, modes analysis, static trim analysis and dynamic gust transient response. This last analysis is compared between both clamped wings, and between clamped and free-flying wings. The aircraft model used for all the analyses is the Common Research Model (CRM) developed by Vassberg et al. (2008). For the last gust comparison however, three different civil aircraft are compared. In the first comparison, a concentrated force of $F = 50000N$ is applied at the wingtip of the plane. In NASTRAN this task is accomplished through the linear static solution sequence (SOL 101). The wing deformation for both software is shown in Figure 5.5. This simulation shows an identical behaviour with just 0.08% difference at the tip, due to minimal modelling differences between the two programs. To complete the validation of the structural analyzer of PROTEUS the modes are calculated and compared using the Modal Assurance Criterion (MAC). In NASTRAN, the normal modes solution sequence (SOL 103) extrapolates the model modes. This comparison method,

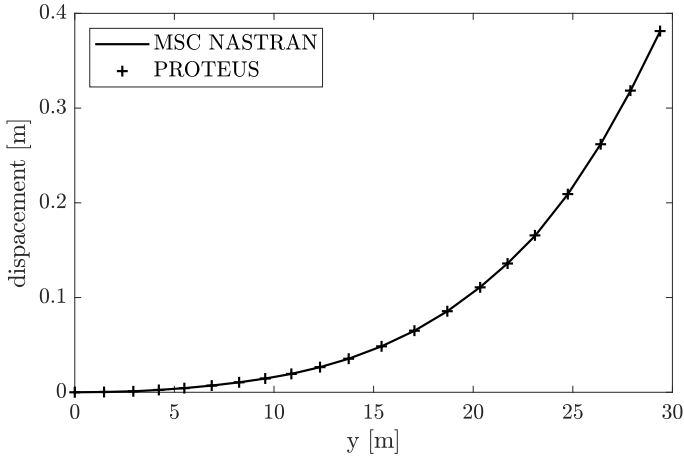


Figure 5.5: Vertical deflection due to concentrated load on the tip comparison.

well explained by Pastor et al. (2012), is an indicator of the degree of consistency between modes shapes. In Figure 5.6, the result of the modes comparison reveals a perfect identity between the modes and their frequencies that is underlined by the diagonal with unity values. The yellow squares suggest a strong correlation between two different mode shapes, and, therefore, a possibility of coupling.

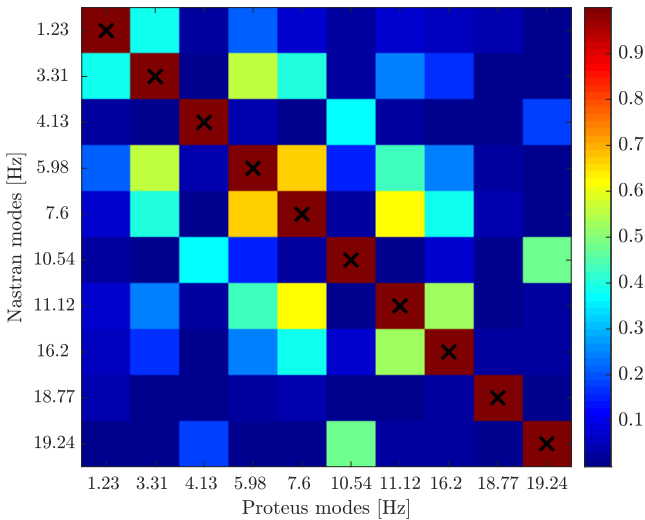


Figure 5.6: MAC for the aircraft structure comparison.

Then a longitudinal trim at horizontal cruise flight condition is computed in NAS-TRAN using the linear aeroelasticity solution sequence (SOL 144), with the purpose of comparing the programs' aerodynamic solutions. In Table 5.2, the trim characteristics are compared. The two software provides the same trim angle, the same wing lift and very similar root bending moment (relative error of 0.98%), with negligible differences due to modelling and measuring errors. In Figure 5.7, the wing lift distribution is compared successfully, with satisfying overlapping of the forces. In Figure 5.8, the displacements of the wing elements regarding longitudinal degrees of freedom (DOF), which are the third and fifth ones, are reported. The third DOF or vertical displacement (Figure 5.8a) shows a difference at the tip of 2.5%. Furthermore, also for the fifth DOF, which is the torsion force around the y-axis (Figure 5.8b), an insignificant difference in behaviour is reported. However, these differences are accepted as the difficulty of having exactly the same model in two different software. Moreover, they have two different potential flow theory methods in aerodynamic modelling (UVLM for NASTRAN and DLM for PROTEUS).

The last type of analysis to be compared is the transient response due to a wind gust

Table 5.2: Trim characteristics comparison.

	MSC NASTRAN	PROTEUS
Trim angle	4.468°	4.453°
Lift (N)	$3.51 \cdot 10^6$	$3.51 \cdot 10^6$
Root Bending Moment (Nm)	$2.30 \cdot 10^7$	$2.26 \cdot 10^7$

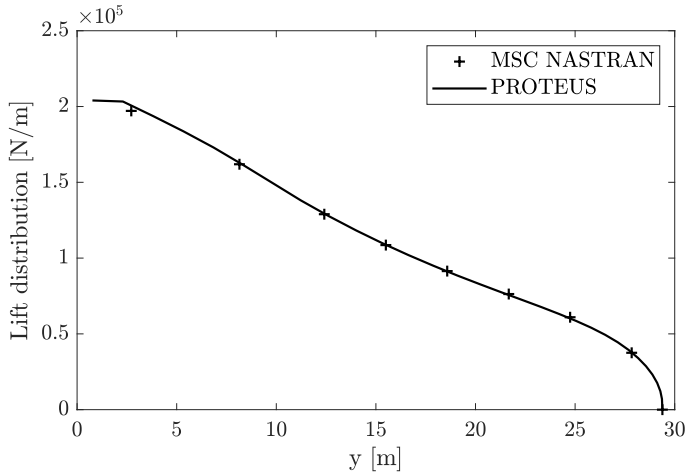


Figure 5.7: Lift distribution comparison.

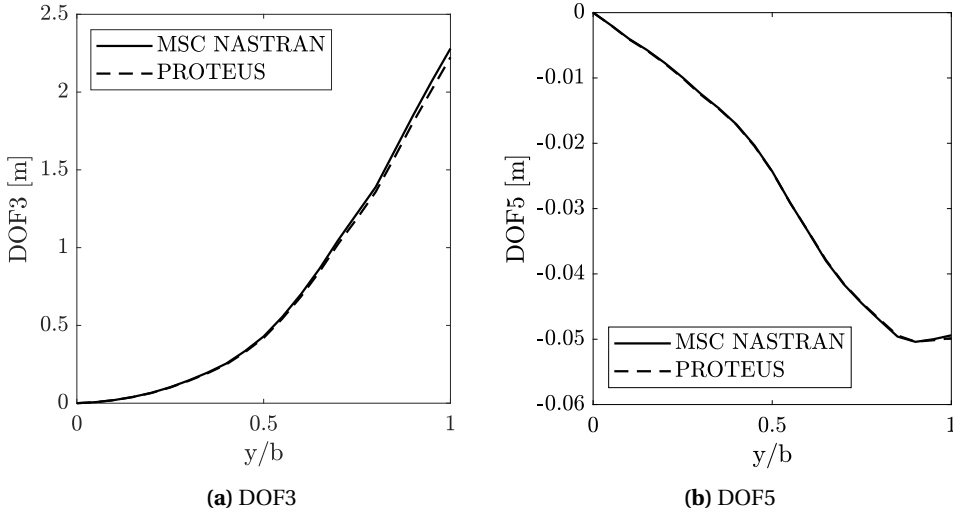


Figure 5.8: Displacement in trim condition comparison.

encountering by the wing. In MSC NASTRAN this analysis is carried out through the dynamic aeroelastic sequence (SOL 146). First, this comparison is executed with a clamped wing. The wing response is shown in Figure 5.9 for a half gust length of $H = 40m$. The comparison reveals very close agreement especially concerning the maximum displacement, with secondary small differences in frequency and damping due to the models using different potential flow methods, as previously mentioned. To have a better un-

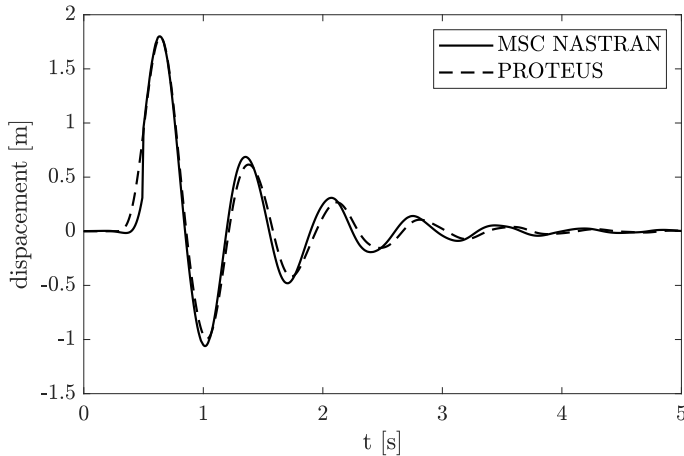
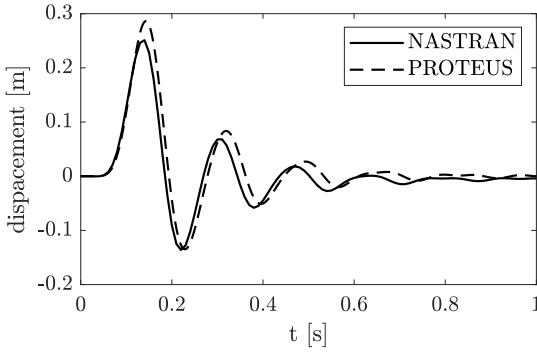


Figure 5.9: Gust response on clamped wing comparison.

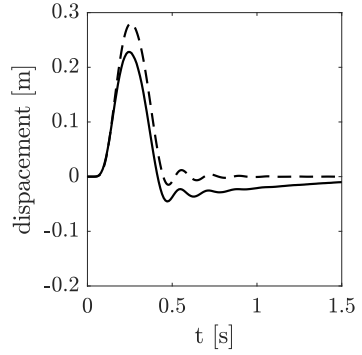
Understanding of the differences between DLM and UVLM results the reader is referred to the work of Wales et al. (2017). Finally, the gust response of a clamped wing in PROTEUS is compared to the same analysis in MSC NASTRAN but considering the wing in free-flying condition, which, in this case, it is recreated by allowing the wing to heave. This comparison is necessary to understand to which extent the optimized design calculated by PROTEUS is affected by this approximation. The analysis is run for three civil aircraft that are the Embraer ERJ-145, the Airbus A-320 and the Airbus A-380, which have a wingspan of 20 m, 35 m, 80m respectively.

In Figure 5.10, the tip displacement is reported for the three different aircraft. For each aeroplane, two short gust lengths are shown as the study revealed that the longest ones produce results more in agreement with each other, especially for the aircraft ERJ-145, in which the length of the long gust is much bigger than its small mean aerodynamic chord and, therefore, the solutions could be considered quasi-steady. It is evident that this approximation is greater for the large A-380, for which the possibility to heave significantly damps the response amplitude for short gusts. For the other cases, it can be appreciated that the responses have almost the same frequencies and damping. However, the general trend is a greater response peak for the clamped wing, as expected since part of the gust is damped by the vertical heaving of the aircraft. The ERJ-145 and the A-320 differ in AR (7.8 and 10 respectively) which explain the greater difference in amplitude as a lower AR means a more compact structure. The Airbus A-380 is the case in which the difference is the most evident. Indeed, for a very large wing, the fact of being constrained in movement reduces the possibility to damp faster the external excitation. Moreover, the frequency of the clamped configuration is very high since the non-optimized model has moderately low modes.

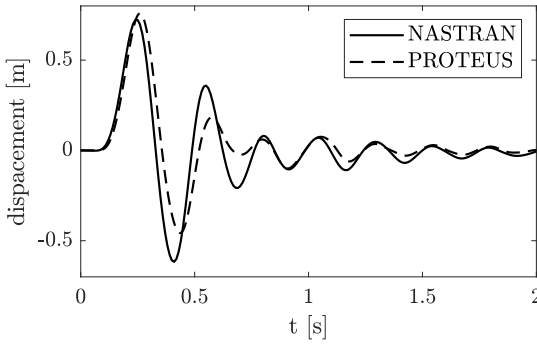
A very clear trend is shown in Figure 3.3, in which the flight envelopes of the three aircraft are compared. In this picture the four main manoeuvres are reported through the root bending (M_x) and torsional (M_y) moments as well as the maximum and minimum moments achieved by the aircraft during the gust encountering of five half gust lengths (10m, 30m, 60m, 90m, 110m). A look at the three charts reveals a difference in the region covered by the gust loads for the three aircraft. For the A-380 (Figure 5.11c) the loads calculated through MSC NASTRAN are less intense than the ones retrieved by PROTEUS regarding both M_x and M_y . Indeed, the maneuver envelope area is increased of 76.6% by NASTRAN gust loads, compared to an augmentation of 124.7% by PROTEUS gust loads. On the other hand, for the ERJ-145 (Figure 5.11a) the loads are smaller in bending moment while still more intense for the torsional one. However, the total load envelope generated by NASTRAN is wider, with an increment in convex area of 51.3%. The A-320 case (Figure 5.11b) is the one in which the loads overlap the most. That means that PROTEUS is generally more conservative in the analysis than a free-flying model-based software, with a great increment factor for the largest aircraft. Moreover, it is also observable that the gust envelope produced by the small and light ERJ-145 is the biggest one in proportion with the manoeuvres, indicating a possible important gust influence in the sizing process. In this case, the convex hull amplifies the maneuver envelope area by 195.73 %.



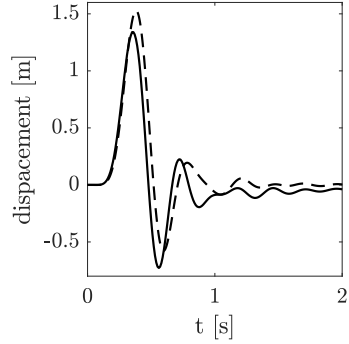
(a) Embraer ERJ-145, L=10m



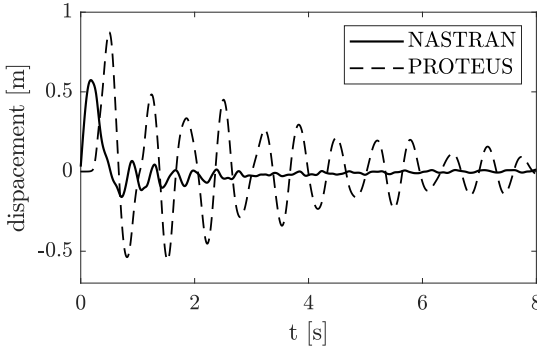
(b) Embraer ERJ-145, L=30m



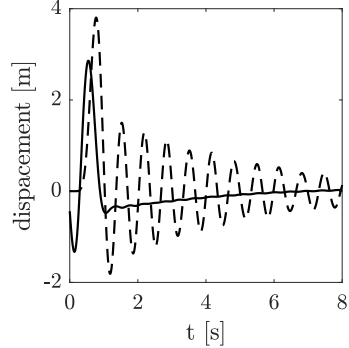
(c) Airbus A320, L=10m



(d) Airbus A320, L=30m



(e) Airbus A380, L=10m



(f) Airbus A380, L=60m

Figure 5.10: Gust response comparison between Free-flying (NASTRAN) and clamped wing (PROTEUS).

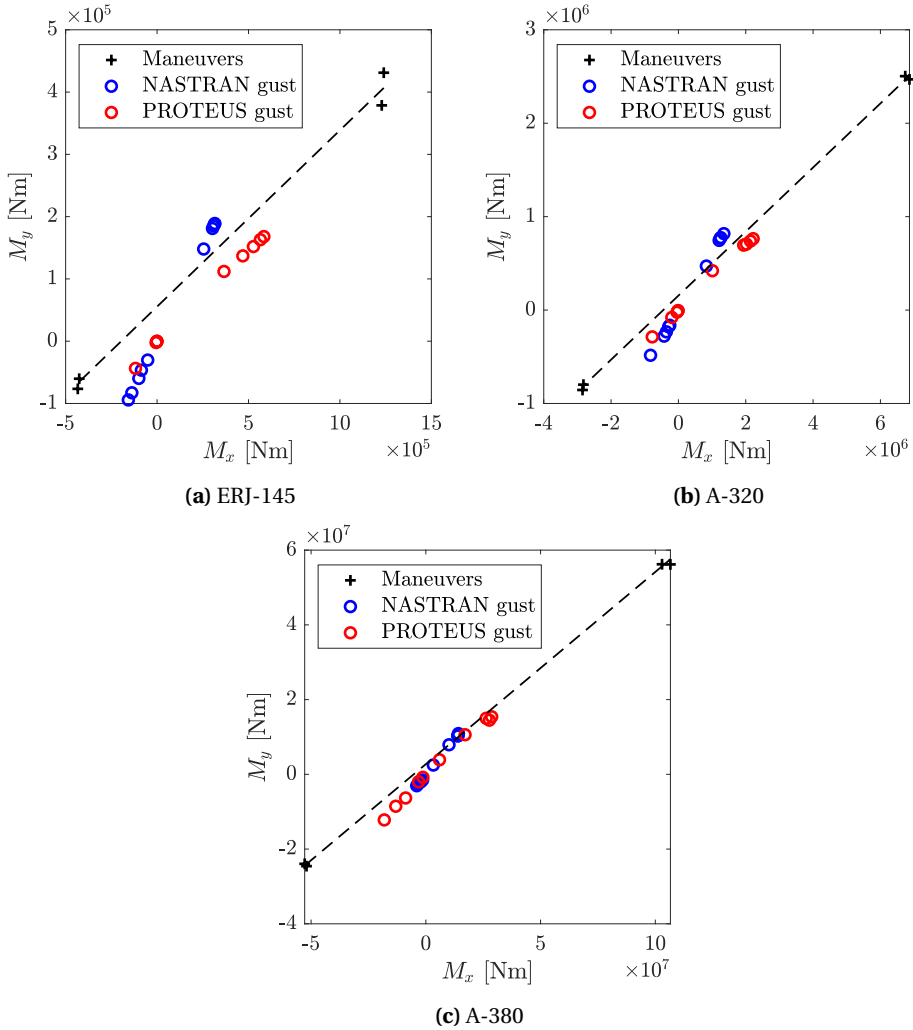


Figure 5.11: Flight envelope for the three aircraft compared.

5.3. OUTER-LOOP OF PROTEUS

The outer-loop of PROTEUS is a modification of the software that allows for an external analysis of the dynamic analysis of the gust response. The purpose of introducing this option is to replicate a common practice in the industrial work environment and to compare it with PROTEUS optimization, which is at the state of the art of aeroelastic optimization. Indeed, designers, which use two different softwares for optimizing and analyzing, usually lose some information in transmitting the data from one program to another. These information are mainly the sensitivities on the dynamic problem, which

are the partial derivatives of the gust response with respect to the lamination parameters and laminate thickness. Sensitivities are an important acquisition for the optimizer to address the best solution to the optimization problem.

In Figure 5.12, the simplified outer-loop structure is reported. The outer-loop branch is initially activated at the beginning of the optimization. An external aeroelastic analysis software (such as NASTRAN) computes the transient response. At this point, the result of the analysis is elaborated before being passed again to the optimization loop. According to the chosen criteria, which are the maximum and minimum wingtip displacement, the maximum and minimum root bending moment and the maximum and minimum wingtip twist, certain time-steps of the response are selected and the Equivalent Static Loads (ESL) are extracted from the solution. The ESL are static loads that reproduce the displacement field obtained by a dynamic load at an arbitrary time. This method was introduced by Cook & Mayne (1980) in civil engineering, but they found fertile ground in aerospace in which the computation time of dynamic analysis and sensitivities is particularly critical for large finite element models. A good review of the several ESL methods is given by Choi & Park (2002). In this case, the ESL are calculated by taking the displacement field \underline{d} at a chosen time t_b and by multiplying it for the stiffness matrix:

$$ESL = \underline{s}(b) = \underline{\underline{K}}_s \cdot \underline{d}(t_b) \quad (5.2)$$

Once the ESL are calculated, they are imported into the optimization loop. Thus, every time the optimizer is required to run the dynamic analysis for the gust response, a static analysis in which the wing is subjected to the ESL is carried out instead. The ESL remain the same until the optimization converges to a value or an arbitrary number of optimization loop has been completed. Then the external analysis is recalled and a new set of ESL are computed.

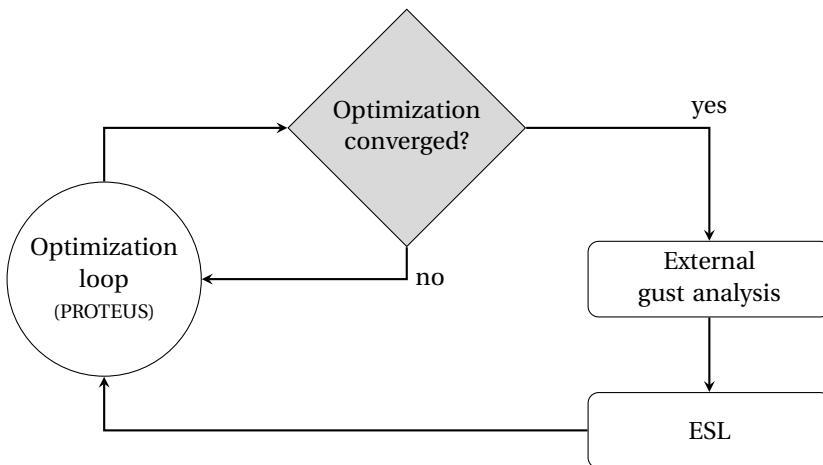


Figure 5.12: Flowchart representing the outer-loop simplified structure.

6

OPTIMIZATION SETUP

This chapter presents the optimization setup used to investigate the influence of gust loads in the aeroelastic optimization of civil aircraft. Since several designs will be performed, the optimization setup is defined not for a particular case, but parametrically depending on the input design parameters of the aircraft generator tool. First, in Section 6.1, the design load cases are presented. Then, the design variables of the problem are explained in Section 6.2, followed by objective, constraint and optimizer choice reported in Section 6.3. Finally, Section 6.4 introduces the reader to several optimization cases that have been explored in this research.

6.1. LOAD CASES

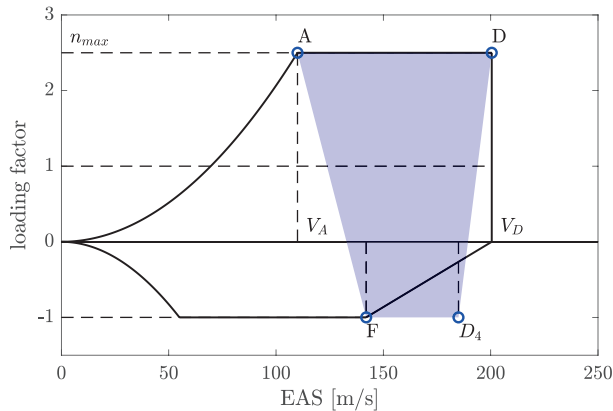
The wing is optimized for four static load cases and a dynamic one. The static load cases are four manoeuvres, two symmetric pull up and two symmetric push-down, while the dynamic one is a $(1-\cos)$ discrete gust response. The four manoeuvres were chosen, in accordance with the certification specifications CS-25 (EASA (2018)), to represent enough points of the manoeuvre envelope while considering several critical altitudes and Mach numbers. In Table 6.1, the parameterized load cases are reported. For each load case, the reference point on the manoeuvre envelope according to the EASA definitions is reported. A typical manoeuvre envelope is shown in Figure 6.1, including in the diagram the static load cases taken into account into this optimization and the area of loads covered between them. The formulae for calculating the parameters indicated in the table are reported in Appendix A. The fuel level is fixed at 0.85, which means 85% of the tank volume, for all the manoeuvres and the gust load cases as a consequence of a preliminary study carried out to find out effects of having different fuel level in the tanks and which outcomes are presented in Figure 6.2. The study shows that there are two opposing trends. On one hand, the relative gust influence on the design diminish by increasing the fuel tank level, as shown in Figure 6.2a in which the percentage indicates

Table 6.1: Load cases (* = derived from EAS/Mach and altitude).

ID	Description	EAS	Mach	Altitude	EASA	n_z	Tank
1	Symm. pull up	V_D	*	6 Km	D	n_{max}	0.85
2	Symm. pull up	V_A	*	3 Km	A	n_{max}	0.85
3	Symm. push down	*	M_c	7 Km	D_4	-1	0.85
4	Symm. push down	*	M_{max}	10 Km	F	-1	0.85
5	Dynamic gust	V_G	*	0 Km	-	1	0.85

the number of design region on the total in which the gust load is the prevalent one. On the other hand, the forces exercised on the wing root increase when the wing tanks are full, as could be seen by the root bending moment (RBM) at different fuel configuration in Figure 6.2b. In the preliminary sizing of a plane, the structural engineer has the duty of making sure that the wing is able to bear the maximum loads that could be faced in the mission. Therefore, a value of 85%, which is the value suggested by regulation C-25.963 for fuel tank testing (EASA (2018)), is chosen to stress the structure as much as possible, taking also into account the low possibilities that an extreme manoeuvre will be faced at full fuel tanks conditions.

As claimed above, the dynamic load case is a (1-cos) gust response. The CS-25 regulation prescribes that the gust is encountered in straight level flight condition, considering enough half gust length between 9 m and 107 m. Therefore, five gust lengths, which are 10 m, 30 m, 60 m, 90 m and 110 m, have been considered in the analysis. Their shape and vertical speed can be seen in Figure 6.3, noticing that shorter gusts have a lower vertical speed. Moreover, the altitude and the speed are chosen to take into account the worst-

**Figure 6.1:** Example of maneuver diagram. In blue the four maneuvers considered.

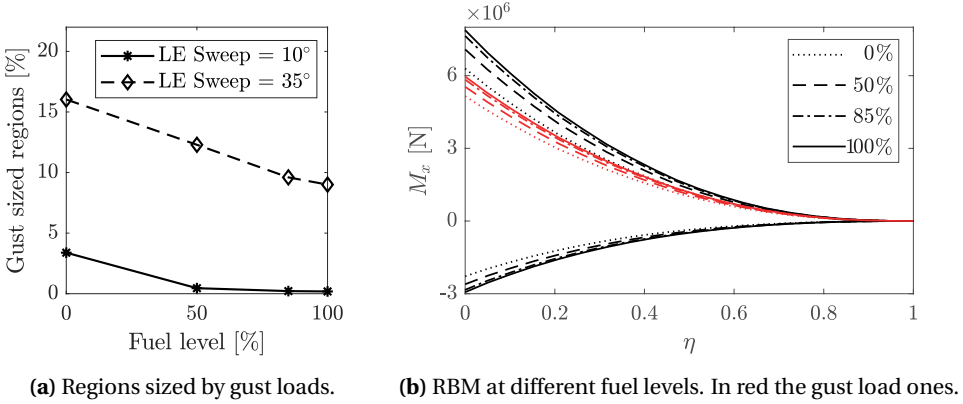


Figure 6.2: Fuel level study for an aircraft with span = 35 m and $MTOW = 75$ tons.

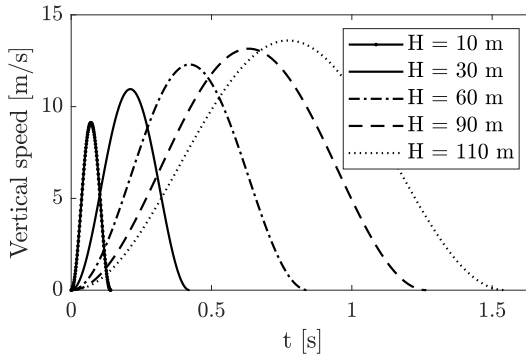


Figure 6.3: (1-cos) gust shape for different half gust lengths.

case scenario, for which the gust encountering is at the maximum speed of the flight envelope at sea level (Werter (2017)). Indeed, the gust amplitude prescribed by certification regulation is higher at sea level and then decreases by increasing the altitudes (EASA (2018)).

6.2. DESIGN VARIABLES

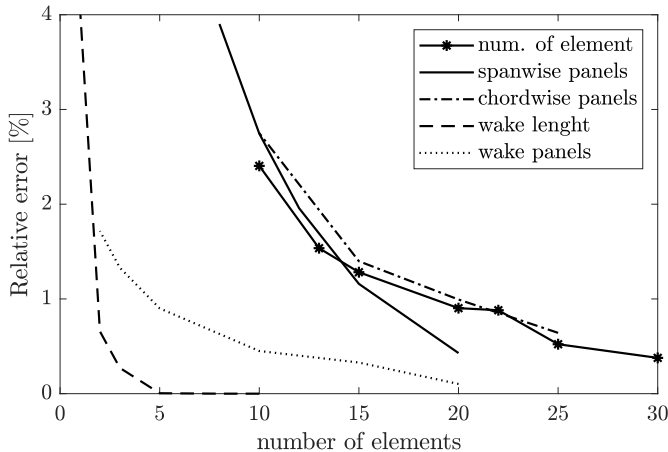
In order to define the accuracy of the structural and aerodynamic discretization, a convergence test is carried out. The purpose of this test is to define the number of panels, elements and the length of the wake to achieve reliable results while keeping the computational time as low as possible due to the high number of optimization cycles required by this research. The convergence test is carried out starting with a high definition model and coarsening it step by step, comparing every time the results with the initial one. This test has been carried out twice, first for a large configuration ($\Lambda_{LE} = 35^\circ$,

Table 6.2: Discretization parameters used to build the aircraft model.

	num. of elements	aero panels chord-wise	aero panels span-wise	wake panels	wake length (in chords)	tip disp. err.
top	30	20	30	10	10	-
used	18	12	18	5	3	1.4%

$MTOW = 375\text{ tons}$, $b = 65\text{ m}$) as well as for one of the smallest producible by the aircraft generator tool ($\Lambda_{LE} = 35^\circ$, $MTOW = 7.5\text{ tons}$, $b = 15\text{ m}$). In Figure 6.4, the results for the convergence test regarding the number of elements, number of chord-wise and span-wise aerodynamics panels, number of wake panels and length of the wake in number of chords is presented. In Table 6.2, a summary of the final quantities chosen compared to the ones used to achieve the finest discretization is given. The chosen discretization leads to an error of just 1.41% in tip displacement with respect to the finest one showing the reliability of the analyses accomplished.

The materials chosen to be compared into the aeroelastic optimization are Aluminium 7075T73 and AS4/8552 carbon fibre epoxy. A composite material is a material system consisting of two or more phases macroscopically, whose mechanical properties are designed to be superior to the ones of the components acting independently (Isaac & Ori (1994)). According to the Classic Lamination Theory, in which the composite is divided into thin homogeneous and orthotropic laminates, the elastic behaviour of multi-directional laminates can be classified into four main categories. First, symmetric laminates, for which each layer on one side of the middle surface has a corresponding layer on the other side, at an equal distance with the same thickness, orientation and proper-

**Figure 6.4:** Convergence study for the discretization parameters.

ties. Second, balanced laminates, for which in the opposite side of the reference plane there are laminates with same properties and thickness, but in which the orientation of the laminates is compensated in pairs from one side to the other and, furthermore, the order of the laminates can be altered. Unbalanced laminates are the most generic configuration, in which neither the orientation is compensated in pairs. Finally, quasi-isotropic, for which the laminates are orthotropic and, thus, the properties are the same in every direction (Dillinger (2015)). The stiffness matrix of a composite material could be written as:

$$\underline{\underline{K}}_s = \begin{bmatrix} A_{11} & A_{12} & A_{13} & B_{11} & B_{12} & B_{13} \\ & A_{22} & A_{23} & & B_{22} & B_{23} \\ & \text{sym.} & A_{33} & \text{sym.} & & B_{33} \\ B_{11} & B_{12} & B_{13} & D_{11} & D_{12} & D_{13} \\ & B_{22} & B_{23} & & D_{22} & D_{23} \\ \text{sym.} & & B_{33} & \text{sym.} & & D_{33} \end{bmatrix} \quad (6.1)$$

in which $\underline{\underline{A}}$ is the membrane stiffness matrix, $\underline{\underline{D}}$ is the bending stiffness matrix and $\underline{\underline{B}}$ is the coupling matrix that establish a connection between in-plane and out-of-plane deformations and loads. In this analysis, the composite with unbalanced laminates will be used to achieve aeroelastic tailoring, while a quasi-isotropic composite will be used as the reference for the unbalanced results. Using a quasi-isotropic composite, the number of design variables decreases since, due to the orthotropic properties of the laminates, $A_{13} = A_{23} = A_{12} = 0$, transforming $\underline{\underline{A}}$ into a diagonal matrix. In PROTEUS, the coupling matrix $\underline{\underline{B}}$ is discarded, and eight laminates parameters are needed to described the stiffness properties of a laminate; four for describing $\underline{\underline{A}}$ and four for matrix $\underline{\underline{D}}$. The characteristics of the materials used in this thesis are reported in Table 6.3.

Finally, the wing is divided into eight design regions, four span-wise and two chord-wise, as illustrated in detail in Figure 6.5. For every design region, the properties of upper skin, lower skin and spars, are calculated. Therefore, there are 24 variables for aeroelastic optimization using Aluminium or quasi-isotropic composite materials since just the thickness of each element for each design region. However, they rise to 216 for aeroelastic tailoring of unbalanced composites because, along with the thickness, the eight laminate parameters that define the stiffness matrix are also required.

Table 6.3: Material properties.

Material	Alluminium 7075T73	Composite AS4/8552
$E_{11}(GPa)$	72.0	128.0
$E_{22}(GPa)$	72.0	9.3
$G_{12}(GPa)$	26.9	4.82
ν_{12}	0.33	0.3
$\rho(Kg/m^3)$	2810	1600

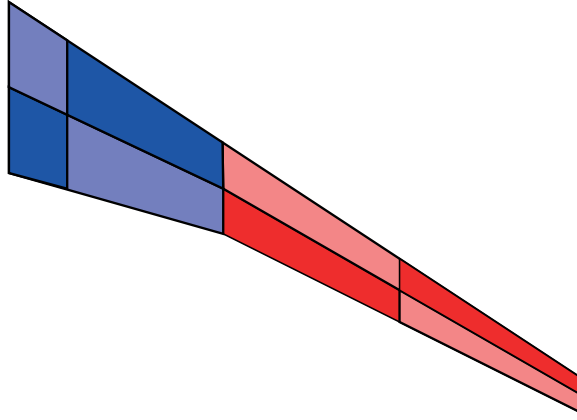


Figure 6.5: Design regions of the wing.

6.3. OBJECTIVE AND CONSTRAINTS

The objective of the aeroelastic optimization is to achieve the minimum weight without violating the constraints. The globally convergent method of moving asymptotes (GCMMA) is a gradient-optimizer, developed by Svanberg (2002), and is used in PROTEUS. As a constraint, a maximum angle of attack is fixed. Buckling analysis is included to avoid structural failure modes. Finally, aeroelastic phenomena are taken into account by considering the first ten critical eigenvalues of the aeroelastic state matrix and checking their stability. A summary of the optimization layout is provided in Table 6.4.

Table 6.4: Aeroelastic optimization setup.

Objective	Minimum weight
Design variables	Laminate thickness Lamination parameters (only for unbalanced composites)
Constraints	Maximum local angle of attack Panel buckling Aeroelastic stability Laminate feasibility Structural strength
Optimizer	GCMMA

6.4. OPTIMIZATION CASES

A total of 165 optimization cases have been carried out in this investigation, occupying a total of 6088 hours that have been managed in parallel computations. The optimization cases can be divided into six different phases of investigation:

1. The fuel inspection phase, in which two aircraft configurations have been optimizing considering four fuel tank levels to be compared with and without the gust load case. Therefore, this first step requires: 2 aircraft x 4 fuel levels x 2 gust/no gust = 16 optimization cases.
2. The first design space exploration phase, in which twenty aircraft configurations were analyzed with the purpose of covering most of the feasible design space. The aircraft analyzed were generated considering three leading-edge sweep angles, three wingspans and for each wingspan two *MTOW*. An additional span has been added for the most swept-back configuration. As before, in this case, the optimization has been compared including and excluding the gust load case. Thus, this phase contains: 20 aircraft configuration x 2 gust/no gust = 40 optimization cases.
3. The deeper design exploration phase, in which 38 new aircraft configurations have been computed to have a better understanding of the behaviour of certain design regions. Among these configurations, ten have been compared with the equivalent case without gust loads. Therefore, in this phase, there are 48 optimization cases.
4. The comparison with outer-loop analysis and static gust load analysis. In this phase, eight configurations have been compared with the designs obtained using the PROTEUS outer-loop and with the ones calculated using a static gust load case, in which the incremental loading factor is retrieved through the Pratt formula. Moreover, the results coming from the six different ESL extraction criteria have been analyzed. Thus, there are: 8 aircraft configurations x 2 outer-loop/static + 5 others ESL criteria = 21 optimization cases.
5. Finally, the composite investigation phase, in which ten designs, which until this phase have been attained using aluminium, are compared to unbalanced and quasi-isotropic composite materials. The unbalanced aircraft are analyzed with and without the gust load case. So, 10 unbalanced configurations x 2 gust/no gust + 10 quasi-isotropic configurations = 30 optimization cases.

As a consequence, 165 optimization cases have been performed. The cases are presented in Figures 6.6, in which the 58 unique aircraft configurations are reported by the input variables used to generate them, which are the *MTOW*, the wingspan and the leading-edge sweep angle. For some of the cases, the further investigations mentioned above are pointed out in both the charts.

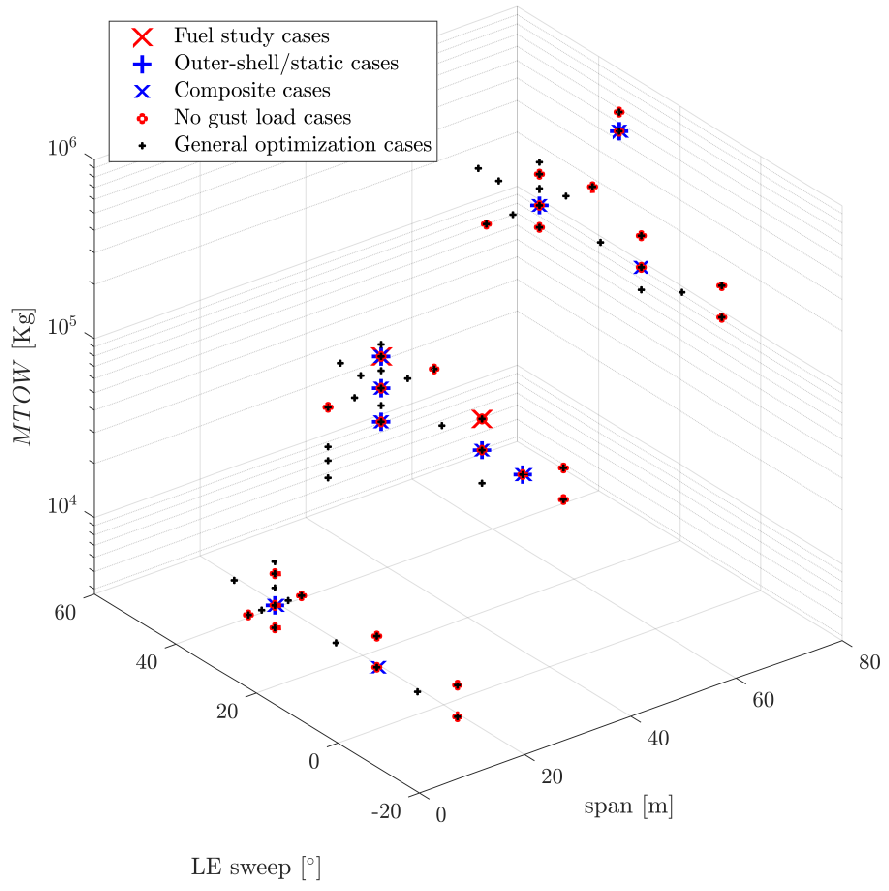


Figure 6.6: Optimization cases analyzed in this research.

7

PARAMETRIC ANALYSIS RESULTS

In this chapter, the findings of the parametric analysis are reported. The results are divided into five categories corresponding to the degrees of freedom on the aircraft design that have been chosen in this research. The first three categories are the general aircraft parameters used to determine each aircraft configuration, which are the leading-edge sweep angle, the wingspan and the maximum take-off weight, presented in Sections 7.1, 7.2 and 7.3 respectively. Then, the material comparison is described in Section 7.4. Finally, the methods in which the gust loads can be included in the aeroelastic optimization are analyzed in Section 7.5. For each category the gust influence on the design is presented and then further explained through detailed charts that sum up findings of several optimization cases. Further results are reported in Appendix C along with the illustration of how the wing shape changes due to each parameter.

7.1. LEADING-EDGE SWEEP ANGLE

In Figure 7.1, the aircraft sensitivity to gust loads is reported as the percentage of the wing lamination regions sized by gust. The percentage of gust sized regions is analyzed by changing the leading-edge sweep angle and keeping the *MTOW* and wingspan constant. The six aircraft configurations analyzed are characterized by three wingspans with two different *MTOW* each. An overall view at the diagram reveals increasing importance of the gust loads in the design when the sweep angle grows. This behaviour is more evident for each wingspan in the heavier configuration cases, which are emphasized by the blue line. This direct correlation can be explained by the aeroelastic damping of the manoeuvre loads at high swept-back angles. Indeed, the deflection produced by a pull-up manoeuvre for a swept-back wing produces not only the bending of the wing, but also a favourable twist distribution. Due to this geometrical property the effective angle of attack of the wing is reduced, especially at the tips. On the other hand, for a forward-swept wing, the opposite happens, resulting in an increasing angle of attack when the

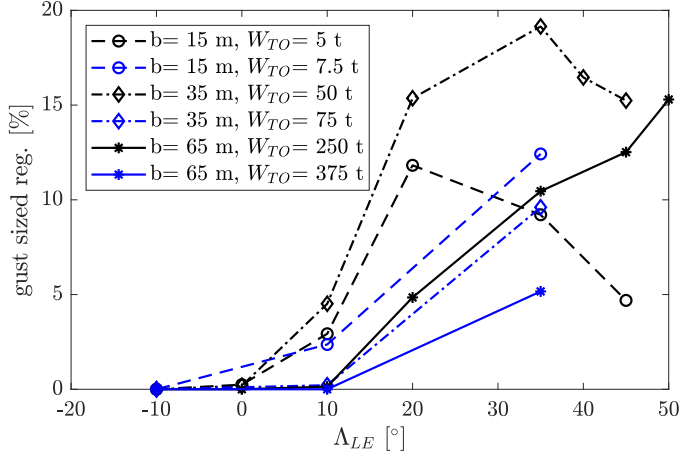


Figure 7.1: Comparison between gust sized regions and leading-edge sweep angle.

wing bends and, therefore, generating critical manoeuvre loads as shown by the zero influence that the gust has when $\Lambda_{LE} = -10^\circ$. The growth of the gust influence encounters however a maximum, located usually between 25° and 35° , which shifts to higher sweep angles for larger aeroplanes. The presence of a maximum could be caused by undesired effects of increasing the sweep angle beyond certain limits. First, the effective beam length increases considerably since the span length is kept constant in the y-axis direction, augmenting the weight of the structural elements. Secondly, by sweeping back the wings, the root torsional moment becomes more and more relevant with respect to the bending one, as shown in Figure 7.3. Finally, when the wing is swept, the wind gust arrives on the wing spanwise sections in different time instants, hitting first the root and then the tip. Thus, the amplitude of the gust intensity is diminished. It is important to add that by increasing the sweep angle of the wing, the design Mach cruise speed also rises, until a maximum fixed at $M_{cruise} = 0.85$ for $\Lambda_{LE} = 37^\circ$ to avoid supersonic velocities.

In Figure 7.2, the normalized structural weight of the wing is analyzed with respect to the sweep angle. The main trend is a slight augmentation in weight when the wing is swept forward and an important rise when the wing is swept back over $\Lambda_{LE} = 30^\circ$. This growing trend is consistent with the theory, in which $W_w \propto 1/(\cos\Lambda)^2$ (Raymer (1992), Torenbeek (2013)). Both the forward and backswept configurations have higher mass mainly due to the increasing torsional forces applied by the loads at the wing root. The torsion M_y is reported spanwise for an aircraft with $b = 35m$ and $MTOW = 50tons$ in Figure 7.3. The parameter η is the spanwise position normalized with the wingspan. The moment distribution is compared between the first load case (LC1) which is a 2.5g pull-up manoeuvre and the gust load case for a half gust length of $H = 30m$ (G30). The manoeuvre torsion is high for both forward and negative sweep angles, while the gust torsional moments always increases with the sweep angle in total intensity. For the neg-

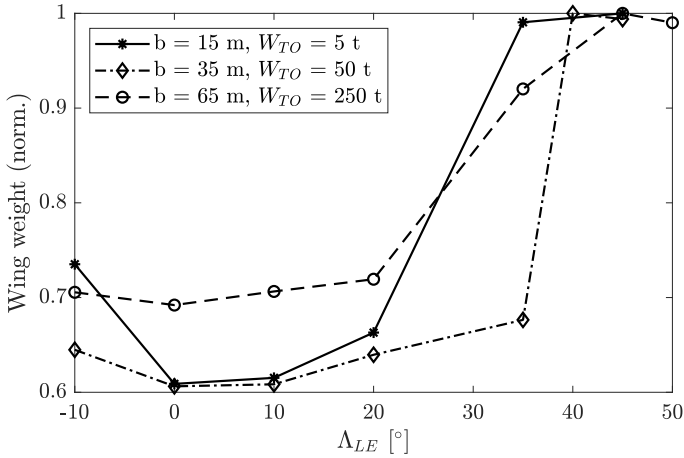


Figure 7.2: Comparison between structural wing weight and leading-edge seep angle.

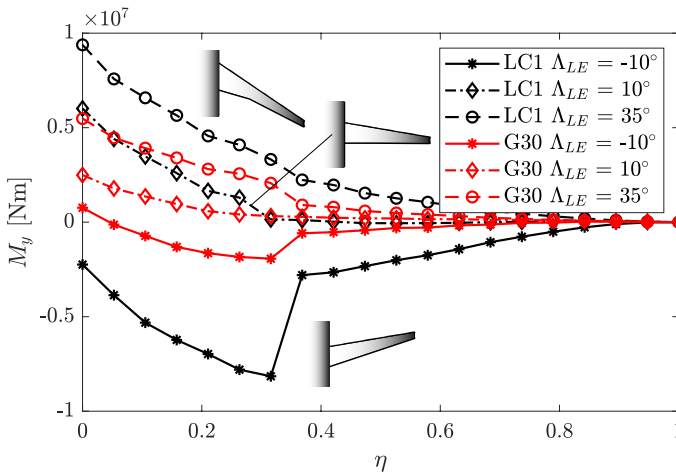


Figure 7.3: Torsion distribution at different Δ_{LE} for $b = 35m$ and $MTOW = 50t$ aircraft.

ative swept wing the torsion is very high due to the bending-torsion coupling effect. The jump at $\eta = 0.3$ is caused by the engine pylon at that location. Situated in front of the leading-edge, the engine position has a greater effect in forward-swept wing as is farther away from the root section elastic axis of the wing.

7.2. WINGSPAN

The second design parameter analyzed is the wingspan. In Figure 7.4, the percentage of regions sized by gust is compared for three different designs by changing the span.

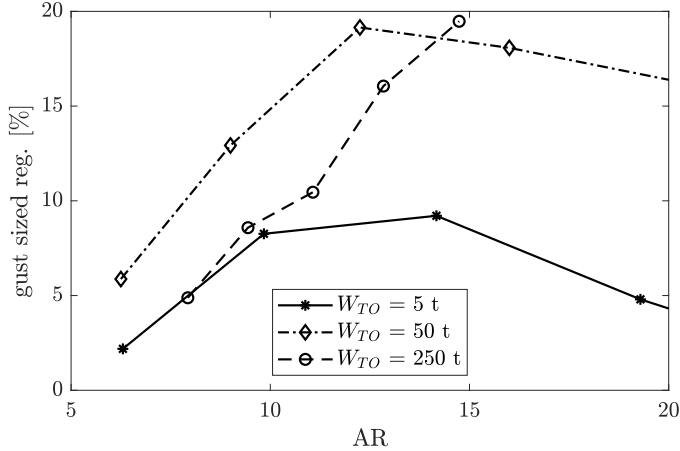


Figure 7.4: Comparison between gust sized regions and aspect ratio ($\Lambda_{LE} = 35^\circ$).

The diagrams feature the aspect-ratio (AR) instead of the wingspan because this parameter is more suitable for comparing properties of aircraft with different sizes. The three configurations are all swept back with an angle of $\Lambda_{LE} = 35^\circ$, following the criticality of high swept wings demonstrated in the previous section. The main findings are that the gust influence gains importance when the AR rises. This growth reaches a maximum at around $AR = 15$ beyond which the increment in wingspan keeping the same $MTOW$ and sweep produces an inverse effect. The growing trend is caused by the fact that increasing the AR the wing is less stiff, as demonstrated in Figure 7.5. In this chart, the bending stiffness is represented by the ratio of the vertical tip displacement (d_{tip}) to the wingspan. The clear tendency is that increasing the AR and, thus, the wingspan leads to an augmentation in d_{tip}/b , which results in a greater flexibility. The lower stiffness is due to having a longer wing for the same weight. A reduced stiffness means lower modes frequencies, which are easily excited by dynamic and impulse loads provoking higher deformation. A closer look at the diagram reveals a lower stiffness at the same AR for the larger configurations. Therefore, considering the same AR a greater wingspan leads to higher deformations due to wind gusts.

The decreasing behaviour of the gust influence for high aspect ratios is also presented as percentage of the regions in which buckling and strain constraints for the gust response exceed a cut off value of 0.6 (the scale is normalized to be 1 the limit of a valid design). The results of this analysis are compared with the AR in Figure 7.6a for the $MTOW = 5t$ configuration and in Figure 7.6b for $MTOW = 250t$. A very clear tendency appears in both cases, with a decreasing number of regions in which gust is sensitive by increasing the AR . However, it is important to remind that the absolute number of regions that overtook the cut-off value does not imply that the gust loads are critical in sizing the aircraft since their importance is relative to the manoeuvre loads constraints. The physical reason for that is that the effect of having the gust encountering the wing

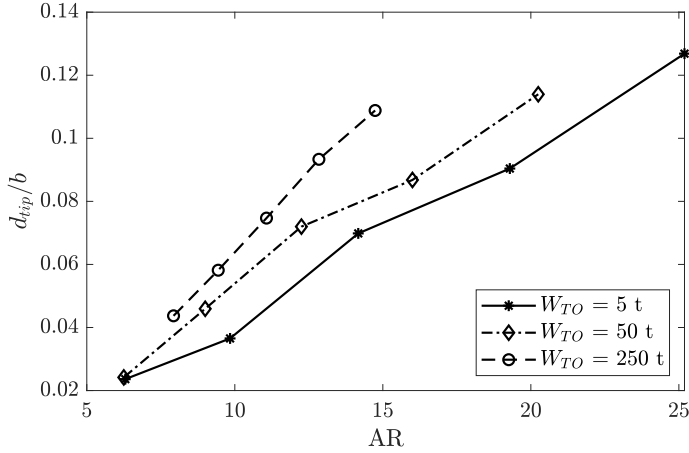


Figure 7.5: Comparison between bending structural stiffness and aspect ratio.

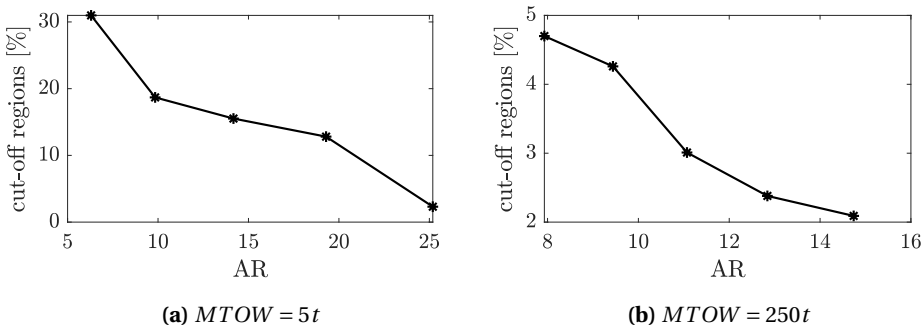


Figure 7.6: Comparison of regions with strain and buckling constraints for gust loads above cut-off value of 0.6 and aspect ratio.

differently spanwise for a swept-back wing is emphasized by enlarging the wingspan.

In Figure 7.7, the flight envelope of an aircraft with $MTOW = 5\text{ t}$ and $\Lambda_{LE} = 35^\circ$ is shown for three different wingspans. By increasing the wingspan, the bending moments of the manoeuvres M_x augment in absolute values. On the other hand, the torsional moment is intensified since enlarging the span provokes the swept-wing to move the centre of gravity point further to the back. Even if changing the span leads to an augmentation of the M_x range covered by the gust loads, their region compared to the manoeuvres one is smaller and more covered by the manoeuvre region. Furthermore, in the diagram, the asymmetry of the gust loads position to the manoeuvre envelope can be noticed. Indeed, only positive gust has been taken into account reducing the number of gust loads by half to save computational time. Moreover, positive gusts are generally more critical

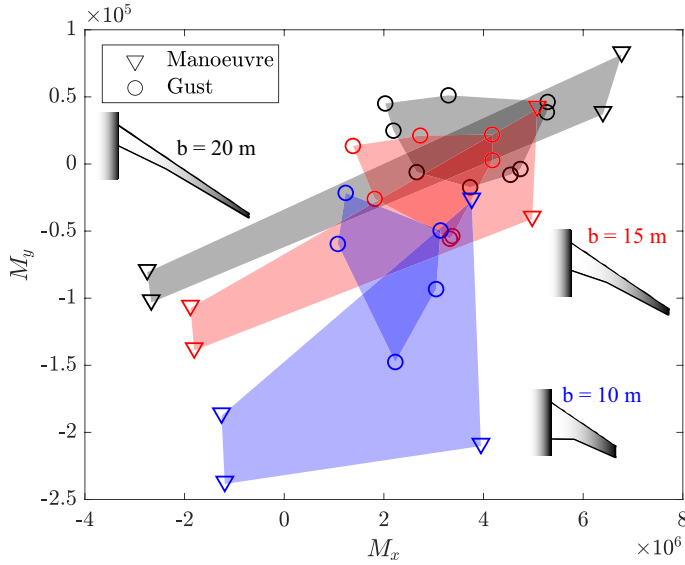


Figure 7.7: Flight envelope of $MTOW = 5 t$ and $\Lambda_{LE} = 35^\circ$ aircraft configuration for three different wingspans.

since they overlap the load distribution of cruise condition, which is also positive being the cruise loading factor 1g.

7.3. MAXIMUM TAKE-OFF WEIGHT

The third design parameter to be analyzed is the maximum take-off weight ($MTOW$). The gust influence is again measured by the number of gust sized regions and it is compared to the maximum take-off weight in Figure 7.8. The main outcome from this analysis is the negative slope of the gust influence line. However, a detailed analysis reveals a behaviour that can be neutral or inverted for the very low $MTOW$ cases. This phenomena could be explained by the direct correlation that exists between maximum take-off weight and wing-loading (W/S), illustrated in Figure 7.9a. Indeed, for a determined configuration with constant wingspan and leading-edge sweep, changing the $MTOW$ results in an increment of the wing loading. Therefore, it can be concluded that an augmentation of the wing loading reduces the sensitivity of the aeroplane to gust loads, in agreement with the studies carried out by Pusch et al. (2019). The only exception has been found in the small design with wingspan $b = 15 m$, for which the high wing loading of the lightest configuration provokes an unusually low number of gust sized regions.

The fact that the gust loads are less critical in sizing the aeroplane when the $MTOW$ decrease below a certain threshold is due to the fact that, in this case, the stiffness of the wing increases considerably, as reported in Figure 7.9b. In this graph, the linear re-

relationship between aspect ratio and the ratio of tip deflection to the wingspan can be observed. The growth of aspect ratio for a constant span implies a decrease of the wing surface area and, thus, of the *MTOW* which is directly correlated to. As a consequence, a higher *MTOW* means a lower *AR*, which implies an high wing bending stiffness and rigidity of the wing. However, dynamic loads have difficulties to excite the rigid wing whose modes are higher. Therefore, it has been shown why the gust influence decreases by increasing the Maximum take-off weight.

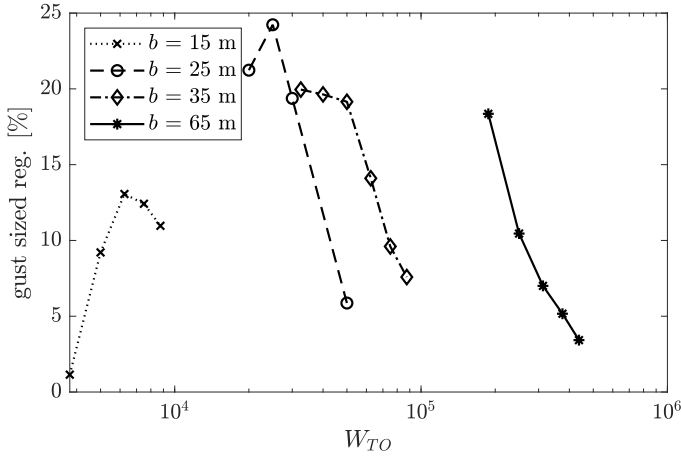
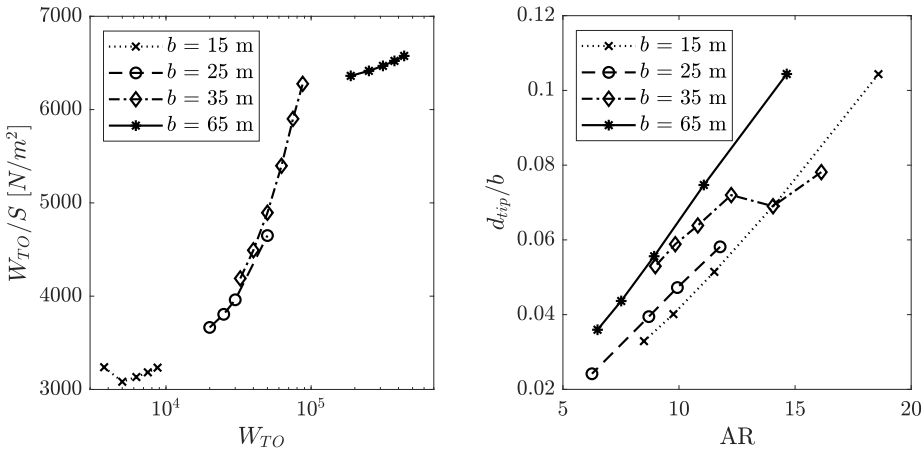


Figure 7.8: Comparison between the percentage of gust sized regions and *MTOW*



(a) Comparison between *W/S* and *MTOW*.

(b) Wing stiffness by changing *AR*

Figure 7.9: Wing characteristics by changing the *MTOW* at constant span and sweep.

7.4. MATERIALS

The material of the wing structure is an important factor in the determination of whether the gust loads play an important role in a specific preliminary sizing process. The chosen materials are three of the most typical designing choice for the aircraft structure. They are aluminium, quasi-isotropic and unbalanced composite, as presented in Section 6.2. The result for each optimization case is reported as the ratio of the wing mass to the aircraft $MTOW$ by changing leading-edge sweep angle (Figure 7.10a), maximum take-off weight (Figure 7.10b) and both wingspan and maximum take-off weight (Figure 7.11). Due to the properties of the material, the composite wings are lighter than aluminium wings. The unbalanced composites aircraft are even lighter because of aeroelastic tailoring effects. The anisotropic properties of the composites are fundamental for lowering bending-coupling effects and alleviating gust response. For this reason, it is possible to notice how the unbalanced composite wings weight diverges from the quasi-isotropic ones when the gust loads are more significant in wing sizing. For instance, in Figure 7.10b while the quasi-isotropic and the aluminium wings have a constant difference in weight, the unbalanced carbon fibre epoxy ones gains a discrete weight reduction at ow $MTOW$, at which the gusts can be more critical as seen in the previous section.

In Figure 7.12, the in-plane stiffness is represented for top and lower wing skins by the circle of stiffness, which represent the stiffness of the material in every direction. In the case of isotropy, the shape is indeed a circle. Otherwise, it has some preferential directions. As it could be seen, the effect of aeroelastic tailoring is changing the lamination properties in order to achieve different stiffness in a different direction depending on the critical loads' distributions. It could be noticed as the root stiffness has the same direction as the wing beams to counteract the heavy pull-up manoeuvres on the top skin

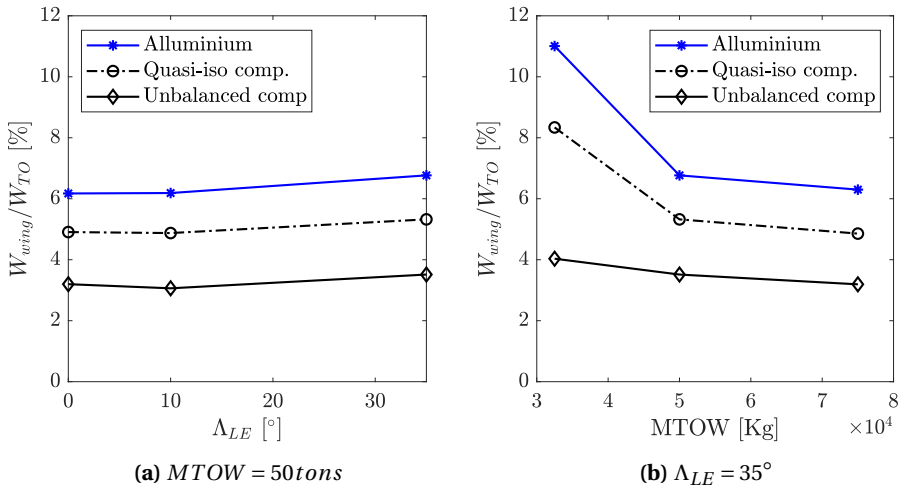


Figure 7.10: Comparison between materials at $b = 35m$.

while to bear push-down manoeuvres for the lower one. The tip stiffness direction on the top skin is aligned with two directions: the y-axis and the chordwise direction. In this way, the stiffness counteracts the torsion and the bending caused by the gust loads, which have a greater influence on this part of the wing.

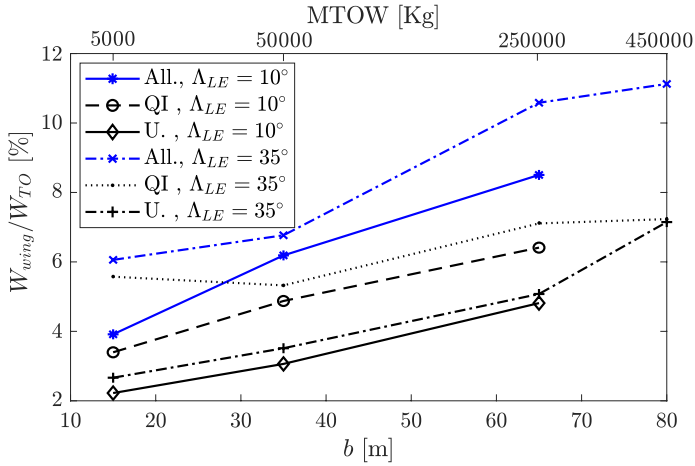


Figure 7.11: Comparison between materials by changing b and $MTOW$.

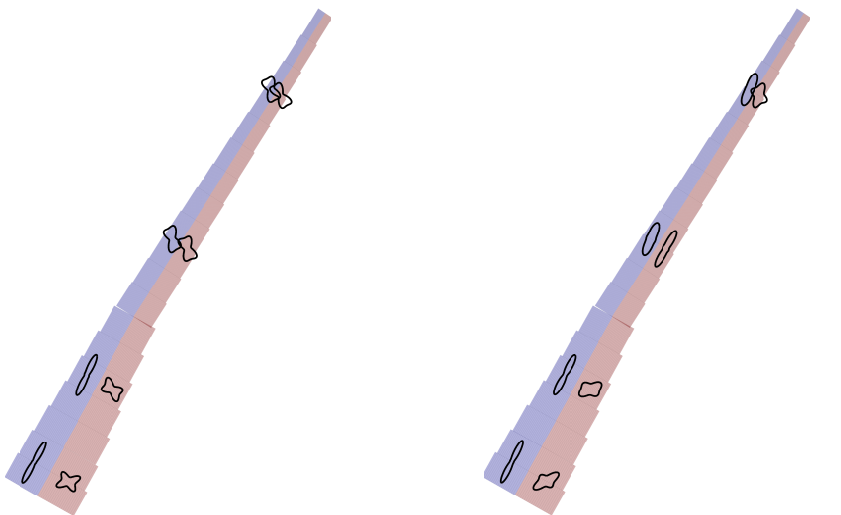


Figure 7.12: Top (left) and lower (right) wing panels in-plane stiffness.

7.5. DIFFERENT GUST ANALYSIS INCLUSIONS

Three different types of gust load inclusion methods have been analyzed. First, the static load, in which the gust is reported as an equivalent incremental loading factor added on the cruise condition and retrieved according to the Pratt formula. Then, the dynamic loads are analyzed, in which (1-cos) discrete gust response is analyzed first in the optimization loop and then in an outer-loop. The results from their comparison are presented here.

The first difference between these three methods could be appreciated in terms of computational time. While the static analysis has taken around 28 hours on average, the outer-loop optimization cases last for 32 hours and the standard PROTEUS optimization with dynamic gust response lasts around 36 hours. These figures have to be analyzed relatively and not absolutely since they depend on several factors, such as the quantity of computational power used or the frequency the external-loop is recalled. However, it is possible to conclude the order in which the methods leads to a growth in computational power with respect to an optimization without gust loads, which generally has lasted for 18 hours. The outer-loop is faster than the dynamic analysis because it is recalled every five optimization loops. When it is not demanded, the static analysis with ESL is carried out instead. The results concerning the time differences between the different models are reported in Table 7.1.

In Figure 7.13, the maximum root bending moment generated by gusts is compared for the three different gust inclusion methods. It is noticed that the dynamic and the outer-loop methods produce similar results, while the static one could generate greater or smaller moment forces depending on the case. However, it is important to underline that none of the static gust load cases have been found relevant as sizing factor. This is due to the fact that even if the static gust generates higher loads, the shape of the loading distribution is the same as a manoeuvre, while in a dynamic case creates a different distribution over imposed on the cruise flight condition. Therefore, in the static case, the gust is covered by higher loading factor manoeuvres.

Finally, in Figure 7.14 the difference between outer-loop and dynamic analysis is reported by the number of gust sized regions and the normalized difference in the wing weight of the two methods. The analysis of the charts reveals the dynamically optimized aircraft are slightly more sensitive to gusts, even if the difference is subtle. Moreover, the final weight of the dynamically optimized wing is heavier than the one obtained with the outer-loop method. The reason for this trend is that the dynamic analysis inside the optimizer gives the sensitivities of the gust response to the design variables. Thus, the optimizer is able to forecast the changing behaviour of the gust response by changing the aircraft characteristics, while for the outer-loop, this information is missing. The difference is even more pronounced when the manoeuvre loads are reduced to 10% of their design values.

Table 7.1: Relative time difference between different gust response inclusion methods.

	No gust	Static	Outer-loop	Dynamic
avarege time (hours)	17.77	27.91	32.08	36.19
time difference	-	+57.1%	+80.5%	+103.7%

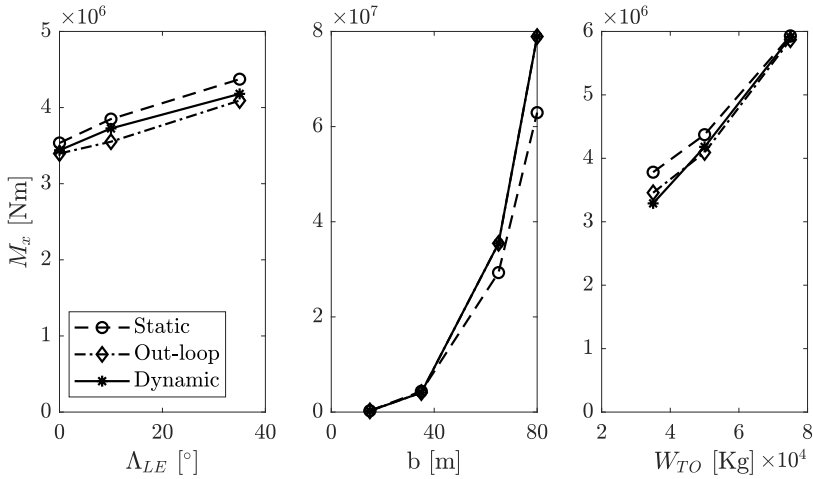


Figure 7.13: Maximum root bending moment caused by gust loads compared between the three different methods of gust load inclusion.

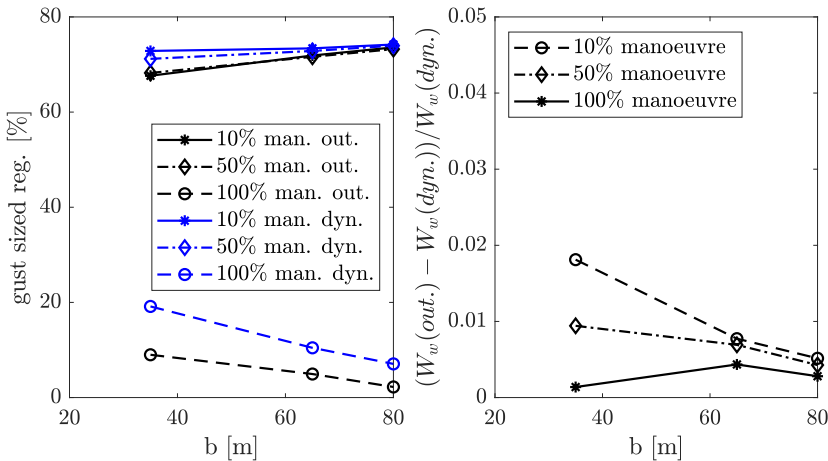


Figure 7.14: Comparison between dynamic and outer-loop optimization by varying the intensity of the manoeuvre loads in regions sized by gust and normalized wing mass difference.

8

DESIGN GUIDELINES AND CASE STUDIES

In this chapter, the design guidelines for gust loads inclusion into aeroelastic optimization of civil aircraft are presented. The guidelines are retrieved from the results presented in the previous chapter. Their presentation and explanation are reported in Section 8.1. An example of their application is then illustrated in Section 8.2, in which two case studies are analyzed and compared to show the accuracy of the predictions made with the guidelines.

8.1. DESIGN GUIDELINES

The guidelines are reported graphically in Figure 8.1 as the expected minimum percentage of the wing structure sized by gust loads. Three parameters have been used to determine each aircraft configuration, namely leading-edge sweep angle, maximum take-off weight and wingspan. For usability, the guidelines are represented in 2D considering just three different leading-edge sweep angles. For each chart, the two axes feature the aspect ratio (AR) and the maximum take-off weight normalized by the square of the wingspan (W_{TO}/b^2). The aspect ratio is chosen over the span since the precise correlation between this dimensionless parameter and the sensitivity of the design to gusts has been demonstrated. The maximum take-off weight is normalized by the wingspan because it has been illustrated that the important factor is not the absolute value of the weight, but its correlation with the aircraft size. Moreover, the span is squared for scaling reasons. The figure is referred to an Aluminium wing with two spars and both main landing gear and engine mounted on the wing. Thus, the values could slightly differ for other configurations. It is important to highlight the fact that the border of the fidelity regions are blurry since their tracing has been carried out from a series of discretized points.

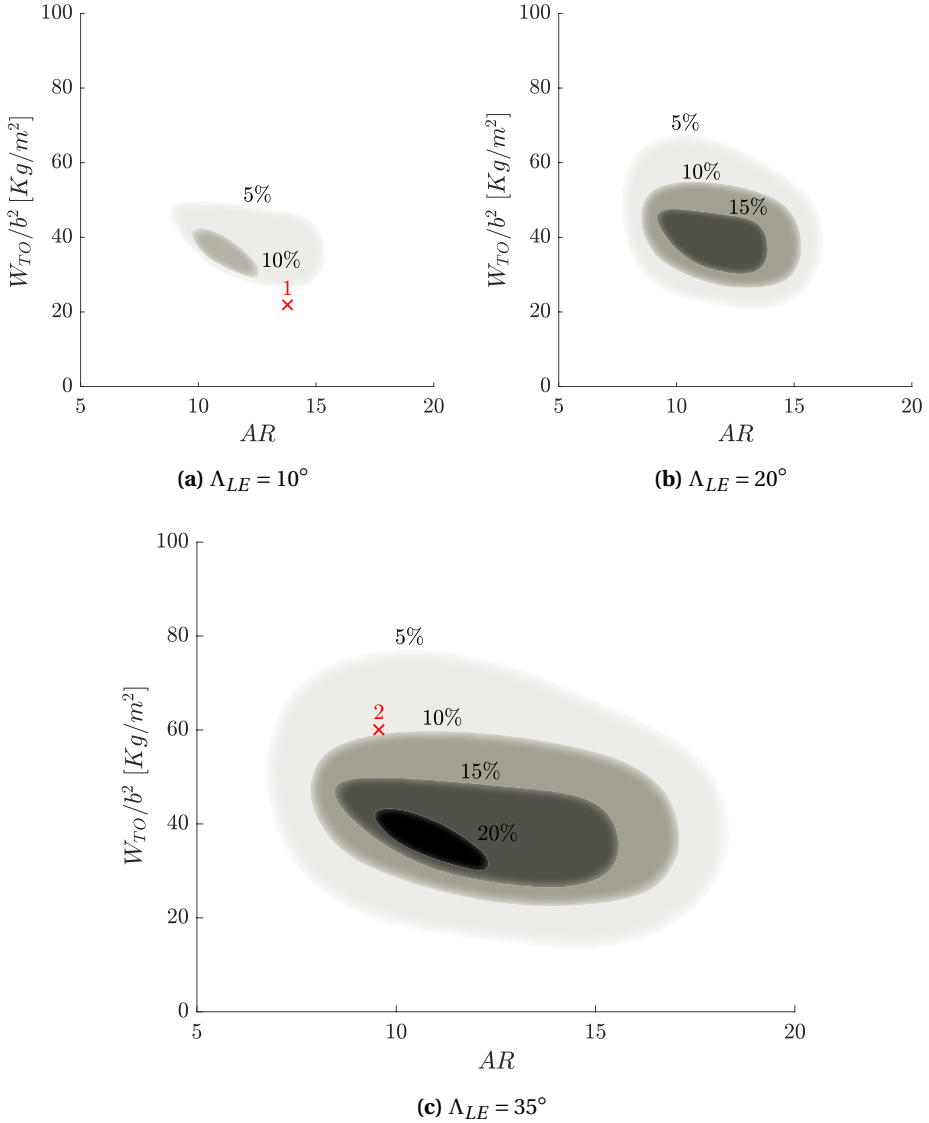


Figure 8.1: Expected percentage of wing structure sized mainly by gust loads depending by Λ_{LE} , AR and W_{TO}/b^2 of the aircraft. In red the two study cases analyzed.

The outcomes of these design guidelines is sum up in the following points:

- By increasing the Λ_{LE} the design sensitivity to gust loads increases, reaching a peak of around $\Lambda_{LE} = 30^\circ \sim 35^\circ$. Swept-forward configurations do not show gusts influence in the sizing process.

- The regions sized by gusts augment by increasing the AR , reaching a maximum between $AR = 10$ and $AR = 13$. Then, they slowly start to decrease again for high AR s.
- The gust sensitivity diminish by increasing the W_{TO}/b^2 ratio. However, when this value is lower than 30, a drop is experienced.
- Composites wing are sized by gust loads for the same parameter triplets. However, when they are sized, the percentage of gust sized regions could grow up to 5% more than the same aluminium values.
- The regions of the wing that are more affected by the gust are close to the wing-tip.
- Having a gust response analysis included in the optimization loop could improve the passive gust alleviation.
- Finally, in case of a gust-sizing situation, the following guidelines are suggested. Above 5%, a preliminary analysis is requested to verify the necessity of dynamic gust response inclusion. In this case, the gust should be at least included as a static load. In case the gust-sized regions are predicted to be over 10% of the wing, the gusts should be considered as dynamic loads and their effect should be taken into account.

8.2. CASE STUDIES

For the purpose of showing the design guidelines application and assessing their efficacy, two case studies are analyzed. The first one is the aeroelastic optimization of a De Havilland Canada Dash 8 Q-200, a turboprop airliner with slightly swept-back wings (data from Bombardier (2006)). The second one regards the design of a Boeing 787-8 Dreamliner, a wide-body twin-engine jet airliner (data from Boeing Commercial Aircraft (2018)). The position of the two cases in the design guidelines is reported respectively in Figures 8.1a and 8.1c. In Table 8.1, the main characteristics of each aircraft are reported along with the comparison between predicted and actual percentage of gust sized regions.

The way of using the design guidelines is illustrated in detail here. Once the main characteristics of the aircraft are retrieved, the derived parameters AR and W_{TO}/b^2 are calculated. Then, the chart with Λ_{LE} closer to the design is chosen. If the actual Λ_{LE} is lower, the area should be considered slightly shrunk. Otherwise, if it is higher than the chart considered, it is expanded. At this point, the prediction on how much percentage of the wing is going to be sized by the gusts could be taken. It is important to remark that in the case of composite wings, the value found should be increased up to 5-10%. Depending on the value found, the conclusion of whether including the gust loads as dynamic loads or not can be taken. In the chart, the comparison between gust size regions predicted through the guidelines and calculated through aeroelastic optimization is pointed out for the two test cases presented before. Looking at the results it is possible to conclude that the design guidelines gives a satisfying prediction on how much

Table 8.1: Case studies data and comparison between predictions and results.

	Dash 8	B-787
Λ_{LE}	3°	35°
b	27.4 m	60.12 m
W_{TO}	16466 Kg	227930 Kg
AR	13.8	9.59
W_{TO}/b^2	21.9 Kg/m ²	60 Kg/m ²
Material	Alluminium	Composites
Predicted gust sized regions	<5%	10% + (5-10% composite)
Calculated gust sized regions	4.08%	20.43%

the gust loads are going to be sizing in a determinant civil aircraft configuration. Finally, in Figures 8.2 and 8.3 the wings and the spars of the two aircraft are reported indicating which load case is the most critical for each laminate. In the figure, the wing appearance of the two models can also be appreciated. As it could be seen, the gust it is sizing mainly in the outer part of the wing, especially for the B-787. Moreover, the top skin and rear part are more sensitive to the gust. Therefore, the rear spar is more sensitive to the gust. It is reasonable to remark in conclusion the importance of considering dynamic gust load case for this aeroplane in order to passively alleviate the load.

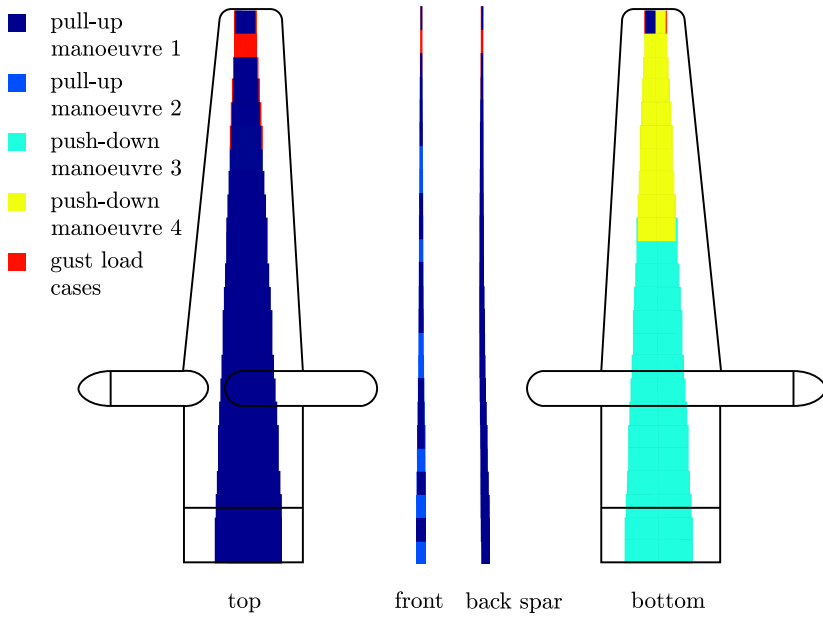


Figure 8.2: Critical load cases for the dynamically optimized Dash 8 wing (buckling).

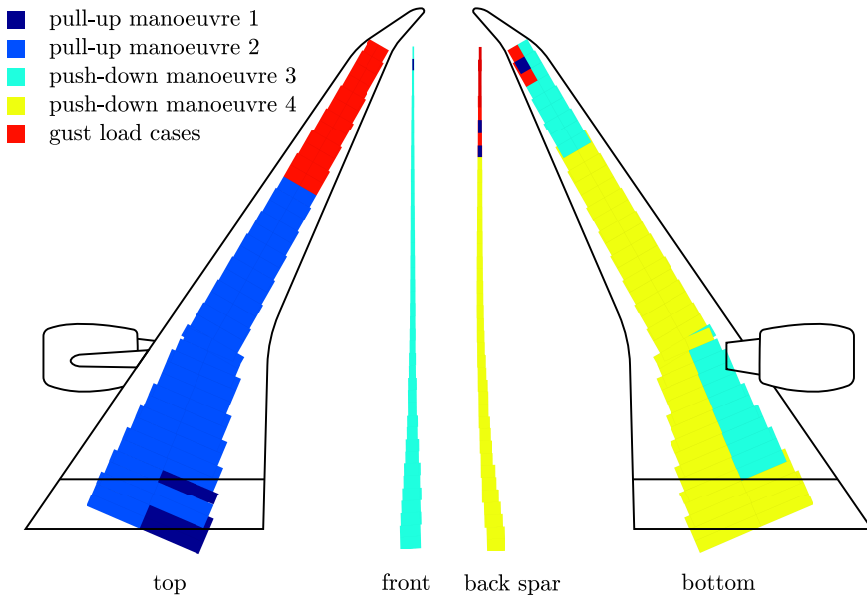


Figure 8.3: Critical load cases for the dynamically optimized Boeing 787 wing (buckling).

9

CONCLUSION AND RECOMMENDATIONS

The inclusion of gust load cases as dynamic load into aeroelastic optimization has been analyzed for several aircraft configurations. It has been shown how their inclusion could be critical and considerably improve the gust response (up to 25% of the civil aircraft wing could be sized for bearing gust loads), while it is just an addition of computational time when the gust loads are not critical. 165 optimization cases have been carried out in the in-house aeroelastic framework PROTEUS exploring different maximum take-off weights, leading-edge sweep angles, wingspans, materials and gust inclusion methods. The results analysis has underlined the strong influence of composite materials on the aircraft gust loads sensitivity. Moreover, the effects of how gusts could become critical also when increasing the wing aspect ratio and the sweep angle, or lightening the structure up to certain thresholds, have been investigated. The possibility of creating design guidelines for gust load inclusion for preliminary sizing of civil aircraft has been demonstrated, presenting a methodological way to assess if a certain aircraft configuration is predicted to be sized by gusts and in which minimum percentage. Two case studies have been finally analyzed to show the application and the efficacy of these guidelines.

The implication of this work for structural engineering research are listed below:

1. It affirmatively answers the question of whether general guidelines for gust inclusion in preliminary sizing could be retrieved.
2. It gives an additional powerful tool to structural engineers to set up the load case choice for an aeroelastic optimization of a generic civil aeroplane, saving time in the preliminary analysis.
3. It quantitatively provides an indication of the sensitivity of the design to gust loads.

4. It enlists elucidations on the gust modelling methods and the different ways to include the gust response analysis in the aeroelastic optimization loop.
5. It helps to avoid waste of computational power in the case the gust loads are not necessary.
6. It provides an aircraft generator tool for retrieving rough civil aeroplane characteristics from three main design parameters.

The recommendations for future works regard further investigations on the topic of this research project. First of all, it would be important to analyze in detail what happens with higher fidelity models in order to retrieve precisely how the gust sizing affects the wing shaping. The addition of control systems and gust load alleviation devices could be included to have a view on the global problem, understanding to which extent the GLA systems and the passive load alleviation are able to improve the gust response. Therefore, the design guidelines could be improved by eliminating those cases in which GLA systems provide enough alleviation to reduce the gust load criticality. Another interesting investigation is seeing the effect of having a free-flying wing in which the relative position of the wing and the horizontal tail varies. Furthermore, the continuous turbulence gust model could be analyzed in order to compare its effects on the aircraft structure with the results obtained with the adopted discrete (1-cos) gust model. Finally, since the load case choice of this research regards a general civil aircraft mission according to certification specifications, different type of mission could be investigated to study the relative influence of gust loads over manoeuvre loads for the structural design of the wing.

A

AIRCRAFT GENERATOR: FORMULAE AND EMPIRICAL STUDIES

In this appendix, laws and empirical formulae with their experimental derivation for the aircraft generator tool are presented.

A.1. TLRs DERIVATION

- **Range (R)**: empirical formula from research on current civil aircraft (Figure A.1).

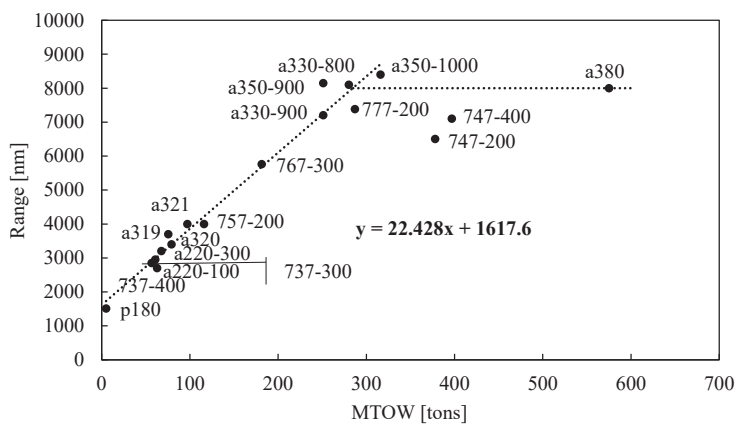


Figure A.1: Experimental formula for Range calculation from MTOW.

- **Cruise Mach speed** (M_{cruise}): linear dependence on Λ_{LE} between three points, $M_{cruise}(\Lambda_{LE} = -10^\circ) = 0.45$, $M_{cruise}(\Lambda_{LE} = 0^\circ) = 0.55$ and $M_{cruise}(\Lambda_{LE} = 37^\circ) = 0.85$. For greater values, constant at 0.875. From M_{cruise} it is retrieved V_c . Then, $V_{max} = 1.15 * V_c$.
- **Stall speed** (V_{stall}): linear dependence on MTOW between two points, which are $V_{stall} = 45m/s$ for $MTOW = 5tons$ and $V_{stall} = 65m/s$ for $MTOW = 575tons$, according to experimental data and typical values shown by Sadraey (2013).

A.2. PERFORMANCES CALCULATION

- **Maximum Wing Loading** ($(W/S)_{max}$): Empirical formula from research on current civil aircraft (Figure A.2).
- **Maximum aerodynamic efficiency** ($(L/D)_{max}$):

$$\left(\frac{L}{D}\right)_{max} = \frac{1}{2} \sqrt{\frac{1}{C_{D_0} K}} \quad (A.1)$$

from Sadraey (2013), in which the zero lift drag coefficient C_{D_0} is calculated using typical values from Torenbeek (2013) among 0.021 and 0.019 depending on the size of the plane and $K = 1/(\epsilon\pi AR)$.

- **Maximum Thrust** (T_{max}):

$$\frac{T_{max}}{W} = \frac{aV_{max}^2}{(W/S)_{max}} + \frac{b}{V_{max}^2} (W/S)_{max} \quad (A.2)$$

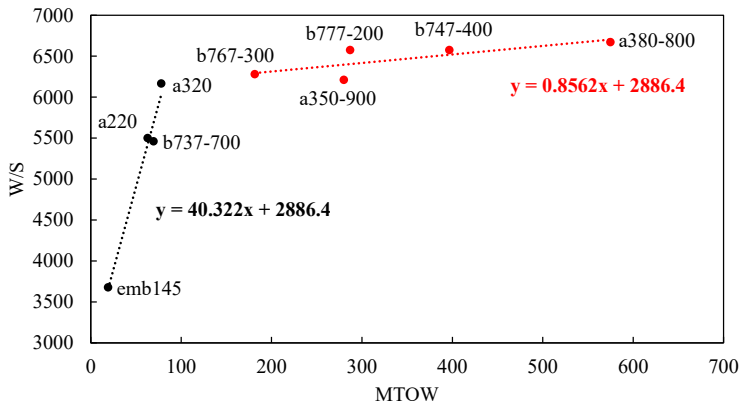


Figure A.2: Wing loading empirical formula.

from Sadraey (2013), in which $a = f(\rho_0, C_{D_0})$ and $b = f(\rho, K)$. The cruise thrust for one engine is retrieved experimentally with $T_{1eng} = T_{max}/8$ and it is needed just for calculating the engine weight.

- **Lift coefficient** (C_L):

$$C_L = \frac{(W/S)_{max}}{\frac{1}{2}\rho V_{max}^2} \quad (A.3)$$

A.3. GEOMETRY CALCULATION

- **Surface** (S), mean aerodynamic chord (mac) and aspect ratio (AR):

$$S = \frac{W_{TO}}{(W/S)_{max}} \quad mac = \frac{S}{b} \quad AR = \frac{b^2}{S} \quad (A.4)$$

- **Taper ratio** (λ): Empirical formula from research on current civil aircraft (Figure A.3).

A.4. WEIGHTS ESTIMATION

- **Fuel Weight** (W_f):

$$\frac{W_f}{W_{TO}} = SF \left(1 - \frac{W_4}{W_3} \right) \quad \frac{W_4}{W_3} = e^{-\frac{R-SFC}{0.866V_c(L/D)_{max}}} \quad (A.5)$$

from Sadraey (2013), in which (W_4/W_3) is the ratio between weight at the end and at the beginning of the cruise and SF is a safety factor that depends by the fact the only the cruise part of the mission is considered fixed at 1.05 .

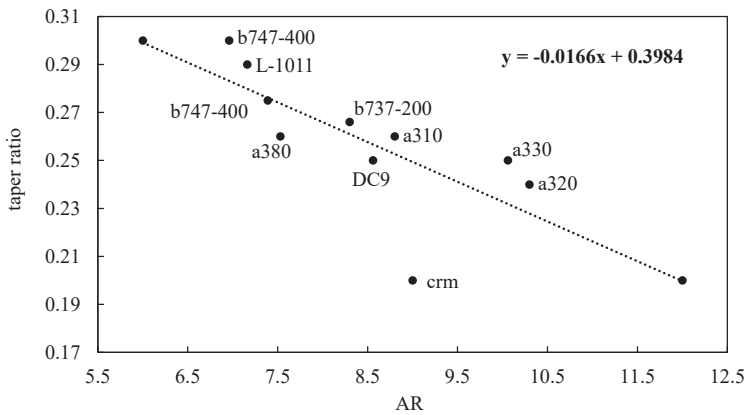


Figure A.3: Taper ratio empirical formula.

- **Empty Weight (W_{ew}):**

$$\frac{W_{ew}}{W_{TO}} = -0.6 \frac{W_f}{W_{TO}} + 0.7 \quad (\text{A.6})$$

extrapolated graphically from the chart reported in Figure A.4 (Torenbeek (2013)) showing empty weight fraction versus fuel fraction for several airplanes.

- **Payload (W_{pl}):**

$$W_{pl} = W_{TO} - W_{ew} - W_f \quad (\text{A.7})$$

derived inverting the unity equation (Sadraey (2013)).

A.5. REST OF THE CALCULATIONS

The rest of the calculations consists of derivations of load cases parameters, mass distribution, fuselage and wing data. To be noticed that load cases formulae are obtained all from the current regulation (EASA (2018)). The main parameters that are used to calculate the load cases described in Section 6.1 are:

$$n_{max} = 2.1 + \frac{24000}{W_{TO}(lb) + 10000} \quad \text{with} \quad 2.5 < n_{max} < 3.8 \quad (\text{A.8})$$

$$V_A = \sqrt{\frac{2q_a}{\rho}} \quad \text{with} \quad q_a = \frac{n_{max}W_{TO}}{C_{Lmax}S} \quad (\text{A.9})$$

$$V_D = 1.25 \cdot V_c \quad (\text{A.10})$$

$$M_{max} = M_c + 0.05 \quad (\text{A.11})$$

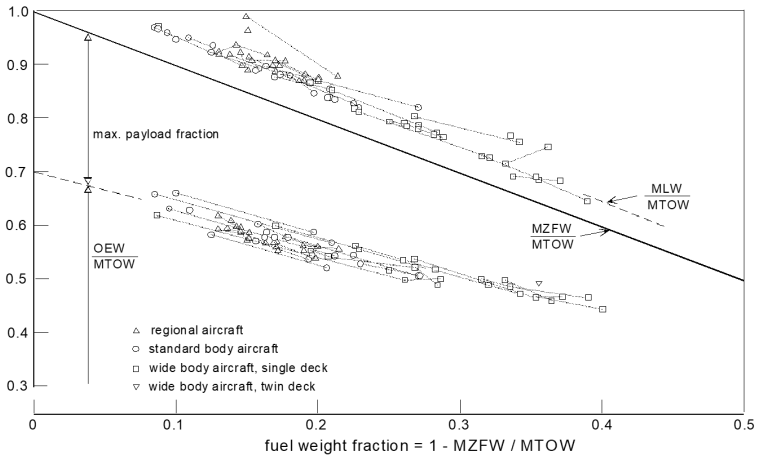


Figure A.4: Empty weight fraction versus fuel fraction (Torenbeek (2013)).

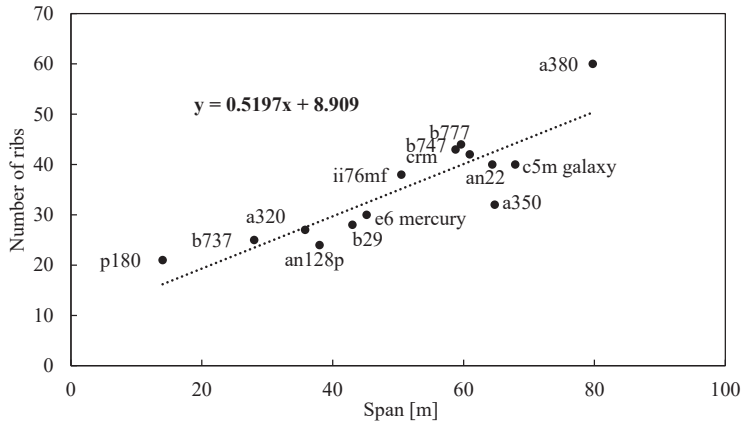


Figure A.5: Number of ribs empirical formula.

Noteworthy laws are the main landing gear (MLG) rule, which changes the shape of the trailing-edge shape of the wing according to the change of leading-edge sweep to maintain a favourable angle to bear the weight of the engine, and the empirical number of ribs rule, depending on linear extrapolation of the aircraft data collected and reported in Figure A.5.

B

OPTIMIZATION CASES LISTED

In this appendix, all the optimization cases carried out in this research are listed in Tables B.1 and B.2. Each aircraft configuration is listed with the types of investigations which has been subjected. For all of the aircraft configurations, an aeroelastic optimization of an aluminium wing subjected to a $(1-\cos)$ dynamic gust load is obtained. Then, for some of these configurations, the types of optimization that have been analyzed are:

- Aeroelastic optimization without the gust load case, marked in the table with the denomination '**No gust**' (one additional optimization case to the configuration).
- Aeroelastic optimization of an unbalanced and a quasi-isotropic wing, marked in the table with the denomination '**Comp.**' (two additional optimization cases to the configuration).
- Aeroelastic optimization with the gust load analyzed externally through the outer-loop and optimization with a static gust load, marked in the table with the denomination '**Out/static**' (two additional optimization cases to the configuration).
- Aeroelastic optimization with four different fuel level, marked in the table with the denomination '**Fuel**' (four additional optimization cases to the configuration).

Table B.1: Optimization cases listed.

ID	$\Lambda_{LE} [^\circ]$	Span [m]	MTOW[tons]	No gust	Comp.	Out/static	Fuel
1	-10	15	7.5	x			
2	-10	15	5	x			
3	-10	35	75	x			
4	-10	35	50	x			
5	-10	65	375	x			
6	-10	65	250	x			
7	10	15	7.5	x			
8	10	15	5	x	x		
9	10	35	75	x			x
10	10	35	50	x	x	x	
11	10	65	375	x			
12	10	65	250	x	x		
13	35	15	7.5	x			
14	35	15	5	x	x	x	
15	35	35	75	x	x	x	x
16	35	35	50	x	x	x	
17	35	65	375	x			
18	35	65	250	x	x	x	
19	35	80	575	x			
20	35	80	450	x	x	x	
21	10	35	32.5				
22	10	65	187.5				
23	0	15	5				
24	20	15	5				
25	45	15	5				
26	35	10	5	x			
27	35	12.5	5				
28	35	17.5	5				
29	35	20	5	x			
30	35	15	3.75	x			
31	35	15	6.25				
32	35	15	8.75				
33	0	35	50	x	x	x	
34	20	35	50				
35	40	35	50				
36	45	35	50				
37	35	25	50	x			
38	35	30	50				
39	35	40	50				
40	35	45	50	x			

Table B.2: Optimization cases listed (Continuation).

ID	$\Lambda_{LE} [^\circ]$	Span [m]	MTOW[tons]	No gust	Comp.	Out/static	Fuel
41	35	35	32.5	x	x	x	
42	35	35	40				
43	35	35	62.5				
44	35	35	87.5				
45	0	65	250				
46	20	65	250				
47	45	65	250				
48	50	65	250				
49	35	55	250	x			
50	35	60	250				
51	35	70	250				
52	35	75	250	x			
53	35	65	187.5	x			
54	35	65	312.5				
55	35	65	437.5				
56	35	25	20				
57	35	25	25				
58	35	25	30				

C

ADDITIONAL RESULTS OF THE PARAMETRIC ANALYSIS

In this appendix, additional results of the parametric analysis are presented. In Figure C.1 the way the parameters change the wing shape when the others are fixed is presented illustratively for clarification. In Figure C.2, the flight envelope for the sweep analysis is reported. In Figures C.3 and C.4, additional results concerning the analysis of the maximum take-off weight are shown. Finally, in Figures C.5 and C.6 further results about the aircraft sensitivity to gust loads are added for the study of different materials for the aircraft structure

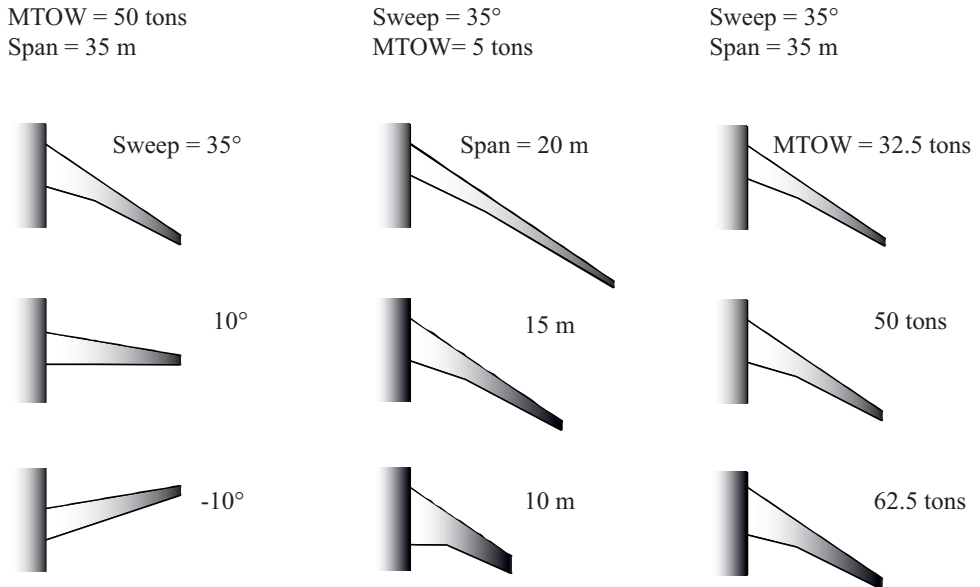


Figure C.1: Illustrative explanation of how the parameters are changed by keeping the other two constant in the aircraft generator tool.

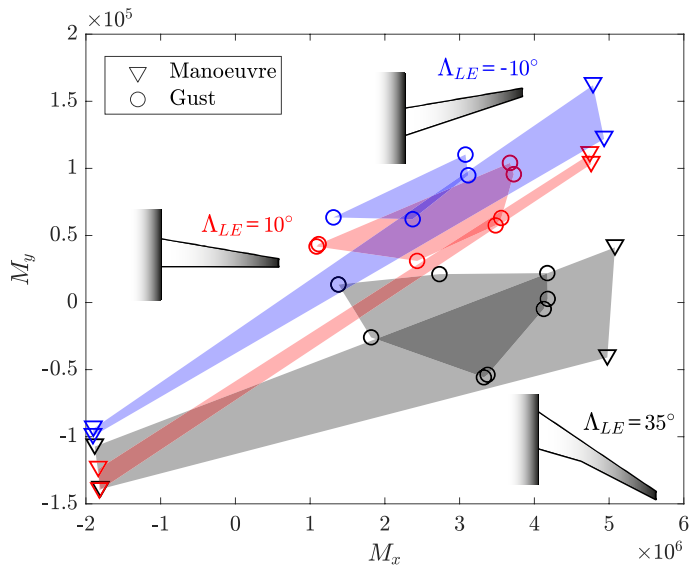


Figure C.2: Flight envelope of $MTOW = 50t$ and $b = 35m$ aircraft configuration for three different leading-edge sweep angles.

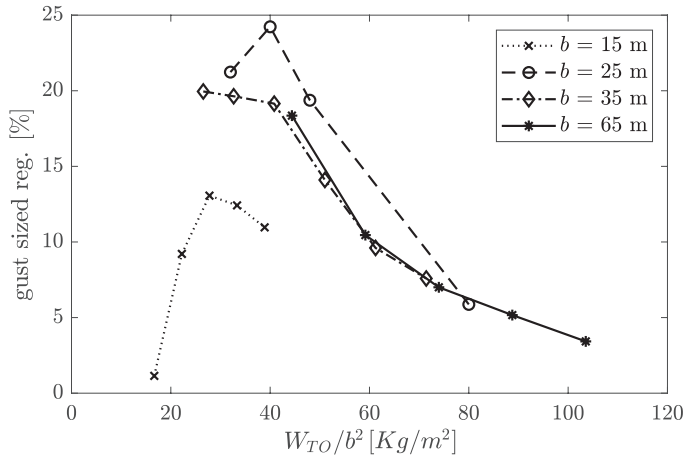


Figure C.3: Comparison between gust sized regions and W_{TO}/b^2 ($\Lambda_{LE} = 35^\circ$).

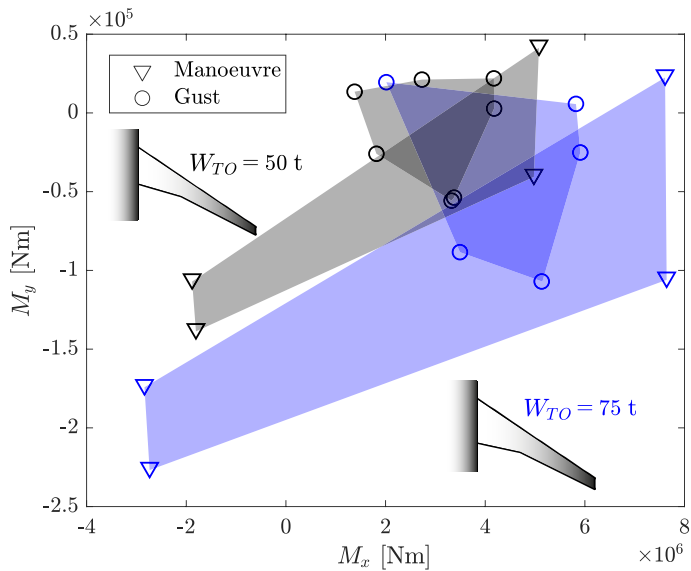


Figure C.4: Flight envelope of $\Lambda_{LE} = 35^\circ$ and $b = 35$ m aircraft configuration for two different maximum take-off weights.

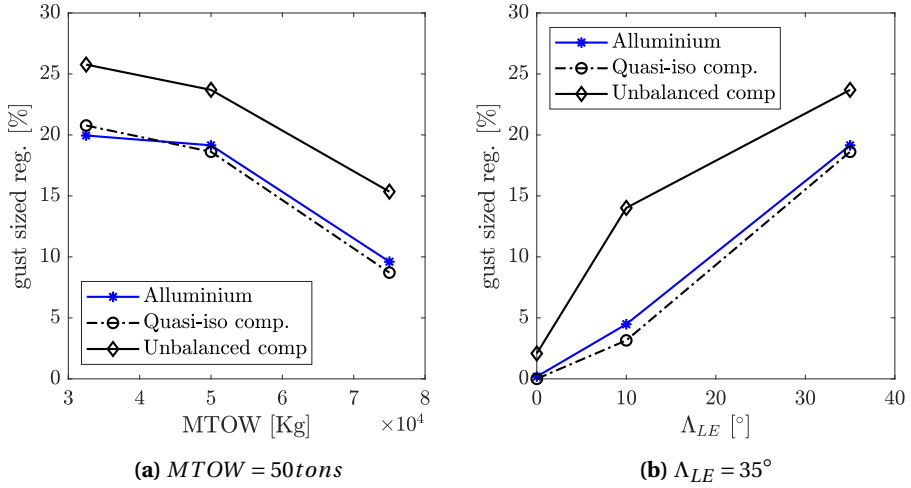


Figure C.5: Comparison between materials at $b = 35\text{m}$ for percentage of gust sized regions.

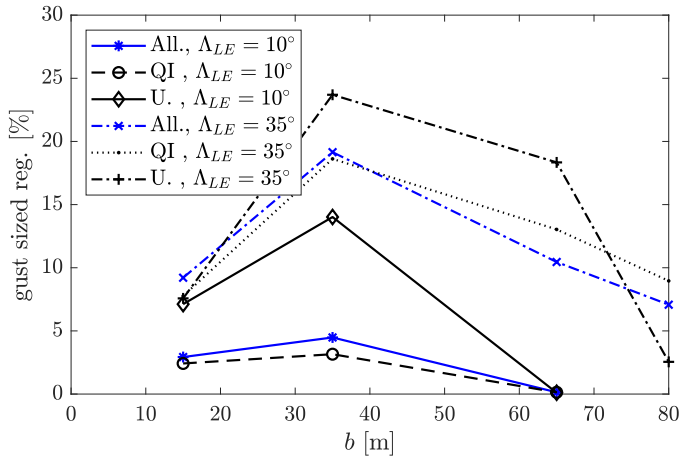


Figure C.6: Comparison between materials by changing b and $MTOW$ for percentage of gust sized regions.

BIBLIOGRAPHY

- Albano, E. & Hodden, W. P. (1969), 'A doublet-lattice method for calculating lift distributions on oscillating surfaces in subsonic flows', *AIAA Journal*, Vol. 7, No. 2, pp. 279-285 .
- Bisplinghoff, R. L., Ashley, H. & Halfman, R. L. (1955), 'Aeroelasticity', *Cambridge: Addison-Wesley* .
- Boeing Commercial Aircraft (2018), '787 aircraft characteristics for airport planning', *Technical Report D6-58333* .
- Bombardier (2006), 'Bombardier Q-200', *Technical Data sheet* .
- Bussemaker, J. H. (2018), 'Wing optimization with active load control', *MSc Thesis project, Delft University of Technology* .
- Chaput, E. (2015), 'Exascale Needs & Challenges for Aeronautics Industry', *www.prace-ri.eu/IMG/pdf/AIRBUS_EricChaput, consulted in May 2019* .
- Choi, W. S. & Park, G. J. (2002), 'Structural optimization using equivalent static loads at all time intervals', *Computer Methods in Applied Mechanics and Engineering*, Vol. 191, pp. 2077-2094 .
- Code of Federal Regulations No. 14 (1988), 'Aeronautics and Space - part 25', *Technical Report, FAA* .
- Cook, N. J. & Mayne, J. R. (1980), 'A refined working approach to the assessment of wind loads for equivalent static design', *Journal of Wind Engineering and Industrial Aerodynamics*, Vol. 6, pp. 125-137 .
- De Breuker, R. (2011), 'Energy-based aeroelastic analysis and optimisation of morphing wings', *PhD Dissertation, Delft University of Technology* .
- De Breuker, R., Abdalla, M. M. & Gürdal, Z. (2011), 'A generic morphing wing analysis and design framework', *Journal of Intelligent Material Systems and Structures*, Vol. 22, pp. 1025-1039 .
- Dempster, J. B. & Arnoldt, J. I. (1969), 'Flight Test Evaluation of an Advanced Stability Augmentation System for B-52 Aircraft', *Journal of Aircraft*, Vol. 6, No. 4, pp. 343-348 .
- Dillinger, J. K. S. (2015), *Static aeroelastic optimization of composite wings with variable stiffness laminates* .
- Disney, T. E. (1977), 'C-5A Active Load Alleviation System', *Journal of Spacecraft and Rockets*, Vol. 14, No. 2, pp. 81-86 .

- D'Vari, R. & Baker, M. (1993), 'A static and dynamic aeroelastic loads and sensitivity analysis for structural loads optimization and its application to transport aircraft', *34th AIAA/ASME/ASCE/AHS/ASC Structures, Structural Dynamics, and Materials Conference, Apr. 19-22, 1993, La Jolla, California* .
- EASA (2018), 'Certification Specifications and Acceptable Means of Compliance for Large Aeroplanes CS-25', *Technical report, EASA* .
- Grihon, S. (2018), 'Structure Sizing Optimization Capabilities at AIRBUS', *12th World Congress on Structural and Multidisciplinary Optimization, Jun. 5-9, 2017, Braunschweig, Germany* .
- Hajela, P. (1986), 'Optimal airframe synthesis for gust loads', *Contractor Report, NASA* .
- Hajela, P. & Bach, C. T. (1989), 'Optimum structural sizing for gust-induced response', *Journal of Aircraft, Vol. 26, No. 4, pp. 395-397* .
- Handojo, V., Lancelot, P. & De Breuker, R. (2018), 'Implementation of active and passive load alleviation methods on a generic mid-range aircraft configuration', *2018 Multi-disciplinary Analysis and Optimization Conference, Jun. 25-29, 2018, Atlanta, Georgia* .
- Harmin, M. Y., Ahmed, A. T., Cooper, J. E. & Bron, F. (2011), 'Aeroelastic tailoring of metallic wing structures', *52nd AIAA/ASME/ASCE/AHS/ASC Structures, Structural Dynamics and Materials Conference, Apr. 4-7, 2011, Denver, Colorado* .
- Hoblit, F. M. (1988), 'Gust loads on aircraft: concepts and application', *Reston: American Institute of Aeronautics and Astronautics* .
- Iorga, L., Malmedy, V., Morris, G., Albani, F. & Polynkin, A. (2016), 'Large-scale optimisation for sizing of aircraft structures subject to fatigue and damage tolerance requirements', *5th Aircraft Structural Design Conference, Oct. 4-6, 2016, Manchester, England* .
- URL:** <http://aerosociety.sds06.websds.net/2018/asdc/slideshows/E-1-slides.pdf>
- Isaac, M. D. & Ori, I. (1994), 'Engineering mechanics of composite materials', *New York: Oxford University Press* .
- Jenkinson, L., Simpkin, P. & Rhodes, D. (2001), 'Civil Jet Aircraft Design: Aircraft Data File', <https://booksite.elsevier.com/9780340741528/appendices/data-a/default.htm>, *Consulted in February 2019* .
- Jutte, C. V. & Stanford, B. K. (2014), 'Aeroelastic tailoring of transport aircraft wings: state-of-the-art and potential enabling technologies', *Technical Report, Nasa* .
- Katz, J. & Plotkin, A. (1991), 'Low-Speed Aerodynamics: From Wing Theory to Panel Methods', *Singapore: McGraw-Hill, Inc.* .
- Khodparast, H. H., Georgiou, G., Cooper, J. E., Ricci, S., Vio, G. A. & Denner, P. (2012), 'Efficient worst case "1-Cosine" gust loads prediction', *ASDJournal, Vol. 2, No. 3, pp. 33-54* .

- Kim, T. U. & Hwang, I. H. (2005), 'Optimal design of composite wing subjected to gust loads', *Computers and Structures*, Vol. 83, pp. 1546-1554 .
- Knoblach, A. (2013), 'Robust performance analysis applied to gust loads computation', *ASDJournal*, Vol. 3, No. 1, pp. 39-50 .
- Leitner, M., Liepelt, R., Kier, T., Klimmek, T., Müller, R. & Schulze, M. (2016), 'A fully automated structural optimization framework to determine critical design loads', *Deutscher Luft- und Raumfahrtkongress*, Sep. 13-15, 2016, Braunschweig, Germany .
- Meddaikar, M. Y., Dillinger, J. K. S., Sodja, J. & De Breuker, R. (2018), 'FLEXOP Application of aeroelastic tailoring to a flying demonstrator wing', *Deutscher Luft- und Raumfahrtkongress*, Sep. 4-6, 2018, Friedrichshafen, Germany .
- MSC Software Corporation (2004), 'MSC Nastran aeroelastic analysis user's guide', *User's Guide*, Version 68 .
- Munk, M. M. (1949), 'Propeller containing diagonally disposed fibrous material', *US Patent*, US2484308-A .
- Neill, D. J. & Herndeen, D. L. (1997), 'Volume I - ASTROS user's manual', *Torrance, California: Universal Analytics* .
- Pastor, M., Binda, M. & Harčarik, T. (2012), 'Modal assurance criterion', *Procedia Engineering*, Vol. 48, pp. 543-548 .
- Patil, M. J., Hodges, D. H. & Cesnik, C. E. S. (2001), 'Nonlinear aeroelasticity and flight dynamics of High-Altitude Long-Endurance aircraft', *Journal of Aircraft*, Vol. 38, No. 1, pp. 88-94 .
- Petersson, Ö. (2009), 'Optimization of aircraft wings including dynamic aeroelasticity and manufacturing aspects', *50th AIAA/ASME/ASCE/AHS/ASC Structures, Structural Dynamics, and Materials Conference*, May 4-7, 2009, Palm Springs, California .
- Petersson, Ö. & Daoud, F. (2012), 'Multidisciplinary optimisation of aircraft structures with respect to static and dynamic aeroelastic requirements', *Deutscher Luft- und Raumfahrt kongress*, Sep. 10-12, 2012, Estrel Berlin, Germany .
- Pettit, C. L. & Grandhi, R. V. (2003), 'Optimization of a wing structure for gust response and aileron effectiveness', *Journal of Aircraft*, Vol. 40, No. 6, pp. 1185-1191 .
- Pratt, K. G. (1953), 'A revised formula for the calculation of gust loads', *Technical Note 2964*, NACA .
- Pusch, M., Knoblach, A. & Kier, T. (2019), 'Integrated optimization of control surface layout for gust load alleviation', *CEAS Aeronautical Journal* **0**(0), 0.
- Rajpal, D. & De Breuker, R. (2017), 'Preliminary aeroelastic design framework for composite wing subjected to gust loads', *International Forum on Aeroelasticity and Structural Dynamics (IFASD)*, Jun. 25-28, 2017, Como, Italy .

- Rao, S. S. (1984), 'Optimization of airplane wing structures under gust loads', *Computers and Structures*, Vol. 21 No. 4, pp. 741-749.
- Rao, S. S. (1986), 'Automated optimum design of wing structures: a probabilistic approach', *Computers and Structures*, Vol. 24, No. 5, pp. 799-808.
- Raymer, D. P. (1992), 'Aircraft Design: A Conceptual Approach', *Washington, DC: American Institute of Aeronautics and Astronautics*.
- Roskam, J. (1985), 'Airplane design, Part I: preliminary sizing of airplanes', *Ottawa, Kansas: Roskam Aviation and Engineering Corporation*.
- Sadraey, M. H. (2013), 'Aircraft design: a systems engineering approach', *Chennai: John Wiley and Sons, Ltd.*
- Schuhmacher, G., Daoud, F., Petersson, Ö. & Wagner, M. (2012), 'Multidisciplinary airframe design optimisation', *28th International Congress of The Aeronautical Sciences, Sept. 23-28, 2012, Brisbane, Australia*.
- Shirk, M. H., Hertz, T. J. & Weisshaar, T. A. (1986), 'Aeroelastic tailoring - Theory, practice, and promise', *Journal of Aircraft*, Vol. 23, No. 1, pp. 6-18.
- Stauffer, W. A. & Hoblit, F. M. (1973), 'Dynamic gust, landing, and taxi loads determinations in the design of the L-1011', *Journal of Aircraft*, Vol. 10, No. 8, pp. 459-467.
- Su, W. & Cesnik, C. E. S. (2011), 'Dynamic response of highly flexible flying wings', *AIAA Journal*, Vol. 49, No. 2, pp. 324-339.
- Svanberg, K. (2002), 'A class of globally convergent optimization methods based on conservative convex separable approximations', *SIAM Journal on Optimization*, vol. 12, no. 2, pp. 555-573.
- Torenbeek, E. (2013), 'Advanced aircraft design: conceptual design, analysis and optimization of subsonic civil airplanes', *New Delhi: John Wiley and Sons, Ltd.*
- Vassberg, J. C., DeHaan, M. A., Rivers, S. M. & Wahls, R. A. (2008), 'Development of a Common Research Model for applied CFD validation studies', *26th AIAA Applied Aerodynamics Conference, Aug. 18-21, 2008, Honolulu, Hawaii*.
- Vio, G. A. & Cooper, J. E. (2008), 'Optimisation of composite Sensorcraft structures for gust alleviation', *12th AIAA/ISSMO Multidisciplinary Analysis and Optimization Conference, Sep. 10-12, 2008, Victoria, British Columbia Canada*.
- Voss, A. & Klimmek, T. (2016), 'Design and sizing of a parametric structural model for a UCAV configuration for loads and aeroelastic analysis', *CEAS Aeronautical Journal*, Vol. 8, pp. 67-77.
- Wales, C., Cook, R. G., Jones, D. P. & Gaitonde, A. L. (2017), 'Comparison of Aerodynamic Models for 1-Cosine Gust Loads Prediction', *International Forum of Aeroelasticity and Structural Dynamics (IFASD)*, Jun. 25 - 28, 2017, Como, Italy.

- Weisshaar, T. A. (1981), 'Aeroelastic tailoring of forward swept composite wings', *Journal of Aircraft*, Vol. 18, No. 8, pp. 669-676 .
- Werter, N. P. M. (2017), 'Aeroelastic modelling and design of aeroelastically tailored and morphing wings', *PhD Dissertation, Delft University of Technology* .
- Werter, N. P. M. & De Breuker, R. (2015), 'Aeroelastic tailoring and structural optimization using an advanced dynamic aeroelastic framework', *International Forum of Aeroelasticity and Structural Dynamics (IFASD)* , Jun. 28 - Jul. 2, 2015, Saint Petersburg, Russia .
- Werter, N. P. M. & De Breuker, R. (2016), 'A novel dynamic aeroelastic framework for aeroelastic tailoring and structural optimisation', *Composite Structures*, Vol.158, pp. 369-386 .
- Wright, J. R. & Cooper, J. E. (2007), *Introduction to aircraft aeroelasticity and loads*.
- Yang, J. S. & Nikolaidis, E. (1991), 'Design of aircraft wings subjected to gust loads: A safety index based approach', *AIAA Journal*, Vol. 29, No. 5, pp. 804-812 .
- Yang, J. S., Nikolaidis, E. & Haftka, R. T. (1988), 'Design of aircraft wings subjected to gust loads: A system reliability approach', *Computers and Structures*, Vol. 36, No. 6, pp. 1057-1066 .
- Yu, Y., Wang, Z. & Guo, S. (2017), 'Efficient Method for Aeroelastic Tailoring of Composite Wing to Minimize Gust Response', *International Journal of Aerospace Engineering*, Vol. 2017, Article ID 1592527 .
- Zhao, Y., Yue, C. & Hu, H. (2016), 'Gust Load Alleviation on a Large Transport Airplane', *Journal of Aircraft*, Vol. 53, No. 6, pp. 1-15 .
- Zotemantel, R. (1993), 'MBB-Lagrange: a computer aided structural design system', *International Series of Numerical Mathematics*, Vol. 110, chap. 8, pp. 143-159 .